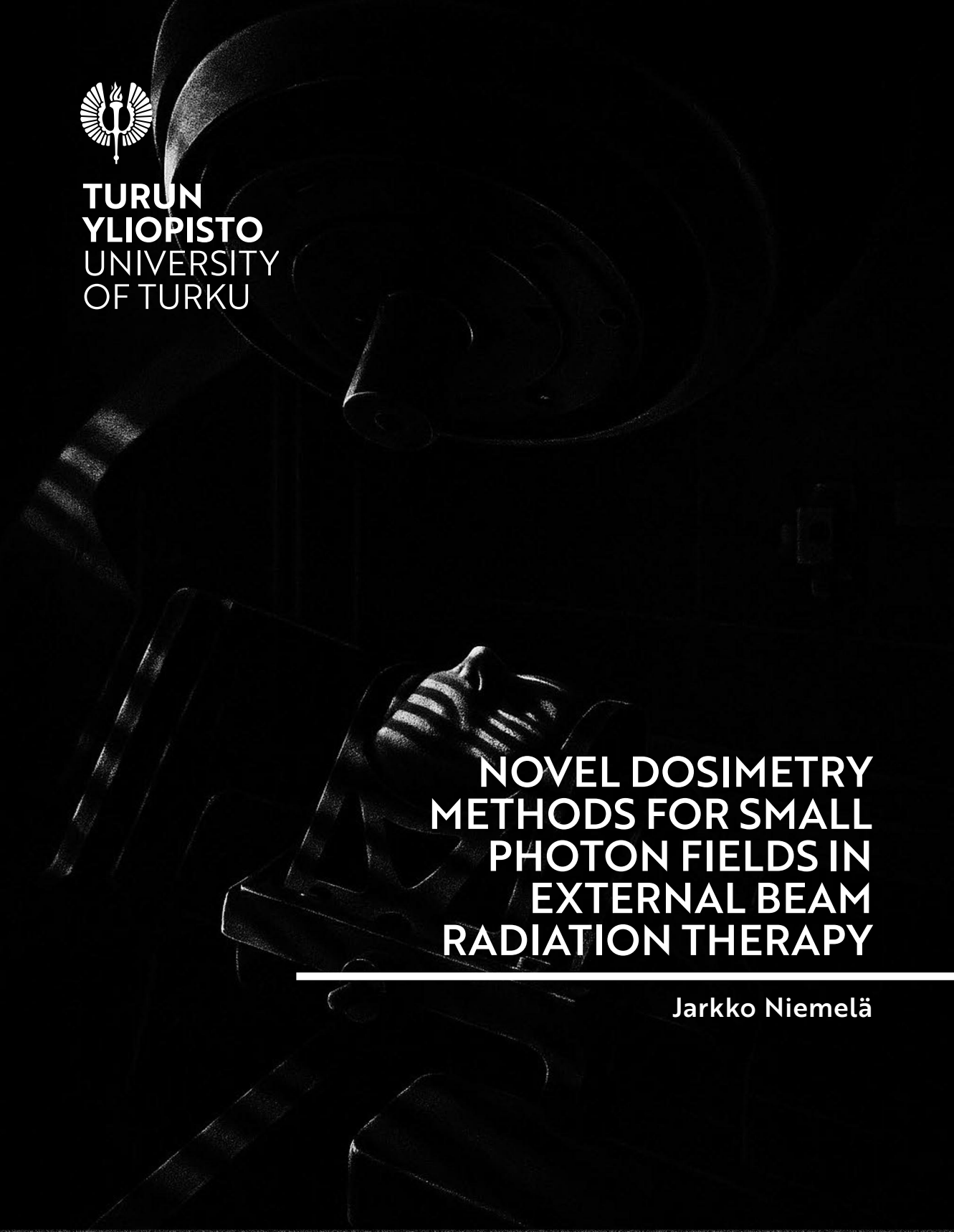

TURUN YLIOPISTO
UNIVERSITY OF TURKU

NOVEL DOSIMETRY METHODS FOR SMALL PHOTON FIELDS IN EXTERNAL BEAM RADIATION THERAPY

Jarkko Niemelä

TURUN YLIOPISTON JULKAISUJA – ANNALES UNIVERSITATIS TURKUENSIS
SARJA – SER. AI OSA – TOM. 734 | ASTRONOMICA – CHEMICA – PHYSICA – MATHEMATICA | TURKU 2025

TURUN
YLIOPISTO
UNIVERSITY
OF TURKU

NOVEL DOSIMETRY METHODS FOR SMALL PHOTON FIELDS IN EXTERNAL BEAM RADIATION THERAPY

Jarkko Niemelä

TURUN YLIOPISTON JULKAISUJA – ANNALES UNIVERSITATIS TURKUENSIS
SARJA – SER. AI OSA – TOM. 734 | ASTRONOMICA - CHEMICA - PHYSICA – MATHEMATICA | TURKU 2025

University of Turku

Faculty of Science
Department of Physics and Astronomy
Physics
Doctoral Program in Exact Sciences (EXACTUS)

Supervised by

Associate Professor Jani Keyriläinen
Department of Medical Physics
Turku University Hospital
Turku, Finland

Associate Professor Jarkko Ojala
Department of Medical Physics
Tampere University Hospital
Tampere, Finland

Reviewed by

Professor Sauli Savolainen
Department of Physics
University of Helsinki
Helsinki, Finland
and
HUS Diagnostic Center (Radiology)
Helsinki University Hospital
Helsinki, Finland

PhD Stéphane Dufreneix
Department of Medical Physics
Institut de Cancérologie de l'Ouest
Angers, France

Opponent

Conjoint Professor Joerg Lehmann
School of Information and Physical Sciences
University of Newcastle
Newcastle, Australia
and
Adjunct Professor
School of Physics
The University of Sydney
Sydney, Australia

The originality of this publication has been checked in accordance with the University of Turku quality assurance system using the Turnitin Originality Check service.

Cover Image: Jarkko Niemelä with DALL·E 3

ISBN 978-952-02-0124-1 (PRINT)
ISBN 978-952-02-0125-8 (PDF)
ISSN 0082-7002 (Print)
ISSN 2343-3175 (Online)
Painosalama, Turku, Finland 2025

For Rahel, Dominic, and Alex—my pillars of strength, my unwavering support, and my endless source of inspiration.

UNIVERSITY OF TURKU
Faculty of Science
Department of Physics and Astronomy
Physics
JARKKO NIEMELÄ: Novel dosimetry methods for small photon fields in external beam radiation therapy
Doctoral Dissertation, 105 pp.
Doctoral Program in Exact Sciences (EXACTUS)
April 2025

ABSTRACT

Small photon beam dosimetry is a critical aspect of modern radiation therapy (RT) techniques, such as stereotactic radiosurgery and stereotactic body radiation therapy. Traditional RT dosimetry methods, designed for standard beam sizes of the order of 10×10 cm^2, cannot be applied to beams smaller than 3×3 cm^2.

This study investigates a novel small cavity point ionization chamber and introduces the dose-area product ratio ($DAPR_{20,10}$) as an innovative parameter for beam quality characterization in small fields. It also addresses challenges like detector perturbation and positioning. Comprehensive experimental and Monte Carlo calculation studies validate the feasibility and accuracy of these methodologies, particularly using large-area plane-parallel ionization chambers and the small-cavity ionization chamber.

The $DAPR_{20,10}$ is found to be largely independent of field size and shape, with certain exceptions, and dependent on beam energy. The results demonstrate that $DAPR_{20,10}$ could be an effective replacement for the traditional beam quality specifier tissue-phantom ratio ($TPR_{20,10}$) in small beam quality specification, offering reduced uncertainties in clinical applications.

The study evaluates field output factors and correction factors for a small-cavity ionization chamber, emphasizing their dependence on photon beam size, energy and detector design. For small photon fields of e.g. 5×5 mm^2, uncertainties due to detector positioning and polarity effects are highlighted, with recommendations for improved measurement accuracy through repeated setups and polarity corrections.

The findings contribute to the advancement of small beam dosimetry, paving the way for standardized methodologies in RT. Future research should focus on further clinical validation, the effect of uncertainties in all steps from the primary standard to dose delivery in a patient, optimizing detector design, and exploring the *DAPR*-based dosimetry protocol to enhance the precision and reliability of small photon beam delivery.

KEYWORDS: radiation therapy, dosimetry, small photon beam dosimetry, beam quality, Monte Carlo calculation, large-area ionisation chamber, small cavity ionisation chamber

TURUN YLIOPISTO
Matemaattis-luonnontieteellinen tiedekunta
Fysiikan ja tähtitieteen laitos
Fysiikka
JARKKO NIEMELÄ: Novel dosimetry methods for small photon fields in external beam radiation therapy
Väitöskirja, 105 s.
Eksaktien tieteiden tohtoriohjelma (EXACTUS)
Huhtikuu 2025

TIIVISTELMÄ

Pienten säteilykenttien annosmittaus eli dosimetria on kriittinen osa modernia sädehoitoa, kuten stereotaktista aivojen tai vartalon alueen sädehoitoa. Tavanomaisiin sädehoitokenttiin (10×10 cm²) sovellettava dosimetria ei ole käyttökelpoinen fotonisäteilykentille, joiden halkaisija on alle 3 cm.

Väitöskirjassa tutkitaan uutta pientä ontelomaista pisteionisaatiokammiota ja annoksen ja-pinta-alan tulon suhdetta ($DAPR_{20,10}$) uudenlaisena parametrina pienten fotonisäteilykenttien säteilylaadun määrittelyssä. Tutkimuksessa käsitellään kyseisen parametrin käyttökelpoisuutta säteilylaadun määrittämisessä sekä ilmaisimen häiriöitä. Menetelmien soveltuvuutta pienten fotonikenttien dosimetriaan vahvistetaan kokeellisten annosmittausten ja Monte Carlo -laskennan kautta.

$DAPR_{20,10}$ -arvon todettiin muutamia poikkeuksia lukuun ottamatta olevan kentän koosta ja muodosta riippumaton, mutta säteilyn energiasta riippuvainen. Tulokset osoittavat, että $DAPR_{20,10}$ voisi korvata perinteisen säteilylaadun määrittäjän ns. kudos-fantomisuhteen ($TPR_{20,10}$) pienissä fotonisäteilykentissä ja siten vähentää muutenkin epävarmuuksia kliinisissä sovelluksissa.

Tutkimuksessa määritellään kenttäkokokertoimet ja niiden korjauskertoimet pienelle pistemäiselle ionisaatiokammiolle korostaen samalla niiden riippuvuutta sekä säteilykentän koosta ja energiasta että ilmaisimen rakenteesta. Pienillä fotonisäteilykentillä (esim. 5×5 mm²) korostuvat ilmaisimen asemointiin ja polariteettiin liittyvät epävarmuudet, mistä johtuen mittaustarkkuuden parantamiseksi olisi suositeltavaa tehdä toistoja ilmaisimen asemoinnin ja polariteettikorjausten suhteen.

Väitöstutkimuksessa saavutetut tulokset luovat perustaa pienten fotonisäteilykenttien annosmittausstandardien kehittämiseksi kliinisessä sädehoidossa. Tulevaisuudessa tutkimusten tulisi keskittyä kliiniseen validointiin, annosmäärityksen kokonaisepävarmuuden määrittämiseen primääristandardista potilaaseen, ilmaisimien suunnittelun optimointiin sekä *DAPR*-pohjaisen dosimetriaprotokollan tutkimiseen ja kehittämiseen.

AVAINSANAT: sädehoito, dosimetria, pienten fotonikenttien dosimetria, säteilylaatu, Monte Carlo -laskenta, suuri tasolevyionisaatiokammio, pieni pistemäinen ionisaatiokammio.

Table of Contents

Abbreviations

2D	Two-dimensional
3D	Three-dimensional
AAPM	American Association of Physicists in Medicine
CAX	Centre-of-axis
CC	Conical collimator
CoP	Code of practice
CPE	Charged-particle equilibrium
CT	Computed tomography
DAP	Dose-area product
DAPR	Dose-area product ratio
FF	Flattening filter
FFF	Flattening filter-free
FOF	Field output factor
FWHM	Full width at half maximum
IAEA	International Atomic Energy Agency
IMRT	Intensity-modulated radiation therapy
IPEM	Institute of Physics and Engineering in Medicine
LAC	Large-area ionization chamber
LCPE	Lateral charged-particle equilibrium
MC	Monte Carlo
MLC	Multi-leaf collimator
msr	Machine-specific reference
MU	Monitor unit
MV	Megavoltage
NTCP	Normal tissue complication probability
OAR	Off-axis ratio
PB	Parallel beam
PDD	Percentage depth dose
phsp	Phase-space
PMMA	Polymethylmethacrylate
PSDL	Primary standards dosimetry laboratory

QA	Quality assurance
RT	Radiation therapy
SBRT	Stereotactic body radiation therapy
SDD	Source-to-detector distance
SI	Système International d'Unités (International System of Units)
SRS	Stereotactic radiosurgery
SRT	Stereotactic radiation therapy
SSD	Source-to-surface distance
SSDL	Secondary standards dosimetry laboratories
STUK	Säteilyturvakeskus (Radiation and Nuclear Safety Authority of Finland)
TB	TrueBeam
TCP	Tumour control probability
TG	Task group
TMR	Tissue-maximum ratio
TPS	Treatment planning system
TPR	Tissue-phantom ratio

List of Original Publications

This dissertation is based on the following original publications, which are referred to in the text by their Roman numerals:

I Niemelä J, Partanen M, Ojala J, Sipilä P, Björkqvist M, Kapanen M, Keyriläinen J. Measurement and properties of the dose–area product ratio in external small beam radiotherapy. *Physics in Medicine and Biology*, 2017; 62(12): 4870-4880.

II Partanen M, Niemelä J, Ojala J, Keyriläinen J, Kapanen M. Properties of IBA Razor Nano Chamber in small beam radiation therapy using 6 MV FF, 6 MV FFF, and 10 MV FFF photon beams. *Acta Oncologica*, 2021; 60(11): 1419-1424.

III Niemelä J, Partanen M, Ojala J, Kapanen M, Keyriläinen J. Dose-area product ratio in external small beam radiotherapy: beam shape, size and energy dependencies in clinical photon beams. *Biomedical Physics & Engineering Express*, 2021; 7(3): 035019.

1 Introduction

1.1 Background

Radiation therapy (RT), chemotherapy and surgery are the most common forms of cancer treatment. The effectiveness of RT depends on the dose-response relationship of cells, which describes how biological tissue reacts to ionizing radiation. Since this reaction is unique to each cell type, the differences between tumour cell and normal cell responses form the basis for determining clinical treatment doses. Clinical dose requirements rely on evidence derived from dose-response curves for tumour control probability (TCP) and normal tissue complication probability (NTCP). These curves typically exhibit a sigmoidal shape featuring a threshold dose, a steep rise and saturation at higher doses.

Alongside advances in technology, the overarching goal of RT optimization is to maximize tumour control while minimizing complications in surrounding healthy tissue. At the steepest points of dose-response curves, small uncertainties in delivered dose can lead to significant changes in clinical outcomes. For instance, a 5% variation in dose can result in 10-20% changes in TCP and 20-30% changes in NTCP. Therefore, accurate dose delivery is crucial: achieving better dose conformity to the tumour while sparing healthy tissue reduces severe side effects and allows for increased treatment doses, ultimately improving survival rates.

This trend has continued over decades, aided by modern imaging techniques that enable the localization of increasingly smaller tumours. However, smaller tumour sizes require proportionally smaller radiation fields, which differ significantly from traditional larger fields in their physical characteristics. This makes the study of small photon field dosimetry in radiation treatment using linear accelerators (linacs) particularly important.

Traditionally, absorbed dose measurements in clinical settings were well defined through standards, including correction factors, with a precision of around ±2% [1, 2]. In static clinical fields comparable to the 10×10 cm² reference field, the determination of absorbed dose and the calculation of dose distribution in patients were straightforward. Early models relied on empirical data, using water as a reference medium with interpolation and extrapolation. Today, treatment planning

systems (TPS) use advanced algorithms to calculate three-dimensional (3D) dose distributions in patients.

Modern RT techniques, such as intensity-modulated radiotherapy (IMRT) [3, 4], image-guided radiotherapy [5] and stereotactic radiosurgery and radiotherapy (SRS/SBRT) [6], have shifted treatment paradigms. Static treatment field sizes of 40×40 cm² to 5×5 cm² are now uncommon, replaced by dynamic fields ranging from 5×5 cm² to less than 1×1 cm², often delivered at higher dose rates. These developments create challenges, as small fields differ fundamentally from the reference field in terms of radiation energy spectrum, mean energy and dose rate. Additionally, the overlap of penumbrae in small fields disrupts charged-particle equilibrium (CPE), complicating the use of traditional measurement protocols [7].

The accurate determination of absorbed doses in small radiation fields is further complicated by the lack of a 10×10 cm² reference field in some modern treatment devices, such as CyberKnife®, Gamma Knife® and TomoTherapy®. These devices require cross-calibration using correction factors to transfer measurement results to reference conditions. Organizations like the International Atomic Energy Agency (IAEA) and the American Association of Physicists in Medicine (AAPM) have been working on protocols for small beam dosimetry; however, these efforts remain ongoing due to the complexity of the task [8].

Uncertainties in small beam dosimetry are larger than in traditional dosimetry, primarily due to perturbation factors in detectors and uncertainties in water-equivalent stopping power ratios. In particular, the Bragg-Gray theory, which underpins dose measurements, is less reliable in small photon fields. For conventional linacs, uncertainties also arise in jaw-defined fields as field sizes decrease [9, 10].

The measured charge in an ionization chamber, used to determine absorbed dose, is influenced by factors such as ion recombination, effective measurement point displacement, wall correction, central electrode correction and perturbation corrections. While these factors are often negligible in larger treatment fields, they become significant in small beam dosimetry due to the absence of CPE. The field size, radiation energy spectrum and detector geometry all affect these correction factors, many of which are not yet fully understood [11, 12].

This thesis investigates small beam dosimetry using two approaches: large plane-parallel ionization chambers and small cavity ionization chambers. For plane-parallel chambers, the absorbed dose can be measured as a dose-area product (DAP), avoiding positional uncertainties associated with point measurements. The ratio of *DAP* measured at 20 cm and 10 cm depths in water, denoted as $DAPR_{20,10}$, is evaluated as a potential beam quality specifier in clinical settings.

For small cavity ionization chambers, the study examines the determination of field output factors (FOF) and associated correction factors. It also explores the feasibility of measuring beam characteristics, such as percentage depth dose (PDD) and off-axis ratios (OAR), comparing results with established detectors. The findings aim to enhance the accuracy and reliability of small beam dosimetry, addressing the unique challenges posed by modern radiotherapy techniques and equipment.

1.2 Application of small photon beams in radiation therapy

Small photon beams are used to treat e.g. melanoma, glioma, brain metastases, and pituitary gland and skull base tumours. Benign targets are mostly meningiomas, acoustic neurinomas and arteriovenous malformations. Small photon beams are used when the target is hard to access or small in size, making it unsuitable for surgical intervention, or when the patient is unwilling to undergo surgery. Beams with diameters of 3 cm or less are considered small in external photon beam RT (**Figure 1**). Measuring the absorbed dose for small photon beams is challenging due to charged-particle disequilibrium, changes to the response of the detector, and volume averaging of the measured dose, since the size of the point detector is similar to the beam.

To accurately determine the absolute absorbed dose delivered by a small beam to a patient, the beam quality must be established and traced back to the primary standard. Achieving this requires measuring the attenuation of the beam. This information is used to translate the absorbed dose in water from a clinic-specific reference field to the settings of the applied small field, or directly to a small clinic-specific reference field. Chapter 1.3 briefly describes how the primary standard of the absorbed dose in water is translated to the absorbed dose in a clinic-specific reference field and, ultimately, in a patient.

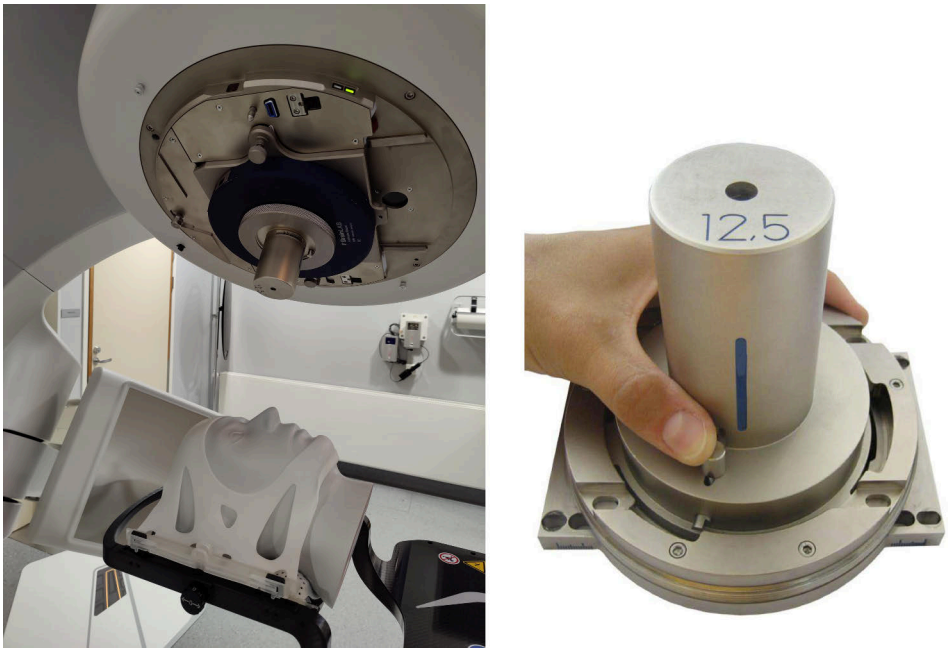

Figure 1. Left: a linear accelerator (linac) with a conical collimator (CC) attached to the treatment head and a phantom positioned on the treatment couch. Right: A CC with an effective diameter of 12.5 mm defined at the linac isocentre (reprinted from [13] with permission from Brainlab AG, Munich, Germany).

1.3 Determining the absorbed dose in a patient

1.3.1 Practical process

To determine the absorbed dose in a patient, one must know the dose delivered by the treatment machine and how the radiation interacts with and is absorbed by the patient. The absorbed dose in water is very close to that in soft tissue, which has a very similar electron density to that of water and accounts for most of the absorbed energy from a high-energy photon beam.

The determination process begins with the primary standard measurement, which serves as the fundamental reference for dose calibration. This standard is maintained by national metrology institutes. Primary standards dosimetry laboratories (PSDL), located in e.g. Paris, Delft and Braunschweig, provide calibrations of reference dosimeters for national secondary standards dosimetry laboratories (SSDL), such as the Radiation and Nuclear Safety Authority of Finland (Säteilyturvakeskus, STUK) in Vantaa. The dose is measured in terms of the absorbed dose to water using highly accurate primary standard ionization chambers or calorimeters. This measurement establishes a baseline for all subsequent dose

measurements. The SSDLs in turn calibrate dosimeters using a water phantom to align secondary standard dosimeters with the primary standard. These secondary dosimeters are then used to calibrate the dosimeters used by hospital personnel. This entire process is called the traceability chain.

The clinical RT equipment, such as a linac, is then calibrated using the dose data from the water phantom measurements. This step ensures that the equipment delivers the correct dose according to the calibration data. Regular quality assurance (QA) checks and recalibrations are conducted to maintain the equipment's accuracy over time. Following linac calibration, the dose absorbed in water can be calculated at a specific distance from the water surface and at a depth correlating to the amount of radiation impinged. The amount of radiation impinged is measured in the linac by a large ionization chamber called the monitor chamber. It is this device that is calibrated against the water phantom measurements traceable to the primary standard, thereby establishing the relationship between linac output and absorbed dose at a specific point in water for a chosen geometry. The monitor chamber measures the radiation exposure, or amount of ionization produced in air by photons from the linac beam delivery system, in Coulombs per kilogramme (C/kg), and this is converted to arbitrary monitor units (MU). The standard practice is to choose 100 MU yielding 1 Gy of absorbed dose at the depth of maximum dose, using a source-to-surface distance (SSD) of 100 cm and a field size of 10×10 cm^2 defined at the water surface.

Each patient undergoes imaging procedures such as computed tomography (CT) or magnetic resonance imaging to create a detailed 3D model of the body. The TPS then uses this model, along with the calibration data, to calculate the dose distribution within the patient. The calculation considers factors such as tissue density, beam energy and treatment geometry to ensure precision in dose calculation.

To verify the accuracy of the planned dose, measurements are often performed with a phantom that mimics the tissues in a human body. If necessary, adjustments are then made to align the delivered dose with the one planned.

During treatment, *in vivo* dosimetry techniques—such as diode or thermoluminescent dosimeter measurements or measuring the exit dose distribution and reconstructing the absorbed dose back to the patient CT scan—may be employed to measure the dose delivered to specific points within the patient's body. This real-time monitoring helps to ensure that the treatment dose matches the planned dose. Any discrepancies detected are addressed either immediately or adjusted for future treatment fractions.

1.3.2 Basic photon beam characterization

The water phantom simulates the human tissue environment, allowing for the measurement of dose distributions at various depths and distances from the radiation source. Three quantities are important for describing the penetration capability of a photon beam. Data obtained from these measurements include *PDD*, the tissue-phantom ratio (TPR) and the tissue-maximum ratio (TMR).

PDD is the ratio of the absorbed dose at a specific depth in water to the dose at the depth of maximum dose, measured along the central axis. *PDD* depends on the SSD, which complicates dose distribution reconstruction.

TPR is the ratio of the dose at a given depth in a phantom to the dose at the same distance from the source but at a reference depth. This reference depth is typically specified to avoid complications from electron contamination. *TPR* is independent of the SSD, making it more practical than *PDD* for dose distribution reconstruction.

TMR is a renormalized form of *TPR* where the reference depth is set at the depth of maximum dose. The main issue with *TMR* is electron contamination at the maximum dose depth, which can affect accuracy. Therefore, using a reference depth further from the build-up region, as in *TPR*, is often preferred for accuracy.

In practice, the simplest form of determining a dose at a given point in a patient is to determine the absolute dose at a depth in water and treat it as an approximation of the dose in patient tissue at the same depth. One can derive this dose when knowing the amount of absolute dose absorbed at reference depth per linac-generated MUs that has been calibrated, and the dose at depth through one of the three quantities *PDD*, *TPR* or *TMR*.

1.3.3 Dose components

Photons from a treatment unit trigger a series of interactions, both within the patient and the treatment unit, before the energy is absorbed as a dose. When the treatment head elements are irradiated, the beam scatters, introducing secondary photons with release of charged particles both in the treatment unit elements and in the air column. These all contribute to the build-up region of the beam in a medium. Dosimetry protocols recommend calibrating beams deeper than this build-up region to avoid this type of particle contamination effect [14].

Photons are indirectly ionizing particles, meaning they do not deposit significant energy directly. Instead, they transfer energy to electrons and positrons through interactions with atoms in the patient, which then ionize and excite other atoms along their paths until their energy is depleted. Based on the interaction history, various dose categories essential for beam characterization and dose modelling can be clearly defined. Most photons entering the patient originate from the electron beam target without prior interactions, contributing to primary and phantom scatter dose

distributions. Interactions in the treatment head create two additional dose categories: charged-particle contamination and head scatter dose. The latter accounts for about 5-15% of the total dose, depending on the beam energy and treatment unit type [15].

2 Aims of the thesis

The aim of this thesis was to study small photon field dosimetry in external beam RT. There were two objectives. First, investigate the feasibility of a new photon beam quality specifier $DAPR_{20,10}$ to determine beam quality to overcome positioning and perturbation uncertainties of a traditional beam quality specifier $TPR_{20,10}$. Second, to study a new small volume ionization chamber for measurements of small beam properties. Particularly, the aim was to understand if $DAPR_{20,10}$ is dependent on beam field sizes and shapes, and how the large area ionization chamber (LAC) affects the measured *DAP* and $DAPR_{20,10}$. These measurements were compared with those of other detectors and Monte Carlo (MC) calculations to verify the LAC measurements. Another goal for this small point-like ionization chamber was to determine the correction factors and FOFs, as well as the basic beam parameters including *PDD* and *OAR* in selected clinical beams, and to compare them with established detectors to advance small beam dosimetry with this potentially feasible energy-independent small ionization chamber.

3 Theory and background

3.1 Absolute dosimetry

3.1.1 Absorbed dose determination

The amount of dose absorbed in a finite volume is determined by the mean energy imparted in this volume [16]

$$D = \frac{d\bar{\varepsilon}}{dm} \quad , \quad (1)$$

where D is the absorbed dose and $\bar{\varepsilon}$ is the mean energy imparted into the mass m in a finite volume. The dose unit is the gray (Gy), or Joules (J) per kilogramme (kg). The ionizing radiation-induced absorbed dose in a volume consists of the energy imparted into, subtracted by the energy exiting, this volume, thereby taking into account all the mass-to-energy conversion in the volume.

3.1.2 International code of practice (CoP)

In 2002, the IAEA, together with the World Health Organization, the Pan American Health Organization and the European Society for Radiotherapy and Oncology, issued a recommendation for dose measurements in external beam RT. This recommendation, titled Absorbed Dose Determination in External Beam Radiotherapy: An International Code of Practice for Dosimetry Based on Standards of Absorbed Dose to Water (IAEA Technical Report Series 398, TRS-398), was revised in 2024 [14].

TRS-398 addresses the fundamental principles of dosimetry for all types of external RT, focusing on photon beam dose measurements under reference conditions. The guidelines and methodology in TRS-398 are centred around the use of absorbed dose to water as the calibration standard, replacing the previously used air kerma standard.

PSDLs have developed experimental techniques to establish the primary standard using calorimetry (graphite or water, as change in temperature). Chemical dosimetry (Fricke dosimeter quantifying the chemical reaction Fe^{2+} -> Fe^{3+} by

absorption spectrometry at an ultraviolet light wavelength of 304 nm) and ionization dosimetry are established through calibration. These are primarily for ^{60}Co gamma ray beams, though some standards also apply to other radiation types such as high-energy photons, electrons and kilovoltage X-rays. The primary standards are based on one of the mentioned methods and ensure consistency in international dosimetry comparisons.

The dose to air can be determined through [14]

$$D_{air} = \frac{Q}{m_{air}} \left(\frac{W_{air}}{e} \right) \quad , \tag{2}$$

where Q is the measured charge, m_{air} is the mass of the air in the chamber, and (W_{air}/e) is the mean energy spent on producing one ion pair in air.

The Bragg–Gray or Spencer–Attix cavity theories then describe how the air cavity dose D_{air} can be converted to dose in medium or dose in water, D_w [14].

The formalism for determining absorbed dose to water in high-energy photon and electron beams using an ionization chamber or dosimeter calibrated in terms of absorbed dose to water in a ^{60}Co beam was detailed by Hohlfeld [17]. Additional work and extensions of this formalism were later developed by Andreo [18] and Rogers [19].

The absorbed dose to water at the reference depth z_{ref} for a reference beam of quality Q_0 in the absence of the chamber is given by [14]

$$D_{w,Q_0} = M_{Q_0} N_{D,w,Q_0} \quad , \tag{3}$$

where M_{Qo} is the dosimeter reading under reference conditions in the standards laboratory and $N_{D,w,Qo}$ is the dosimeter calibration factor in terms of absorbed dose to water, obtained from the standards laboratory. In clinical settings, the measurement conditions often differ from the reference conditions used in the standards laboratory, which can influence the dosimeter response. Therefore, it is essential to account for the differences between reference conditions and the clinical measurement conditions when determining the absorbed dose.

Reference conditions for calibrations in terms of absorbed dose-to-water include factors such as the geometrical setup (distance and depth), field size, the material and dimensions of the irradiated phantom, and environmental conditions like ambient temperature, pressure and relative humidity.

When a dosimeter is used in a beam of quality Q, which differs from the calibration beam quality Q_0, the absorbed dose to water is calculated as [14]

$$D_{w,Q} = M_Q N_{D,w,Q_0} k_{Q,Q_0} \quad , \tag{4}$$

where M_Q is the dosimeter reading corrected for reference conditions, $N_{D,w,Qo}$ is the calibration factor in terms of absorbed dose-to-water for the reference beam quality

Q_0, and k_{Q,Q_o} is the correction factor that accounts for differences between the reference beam quality Q_0 and the actual beam quality Q.

The beam quality correction factor k_{Q,Q_o} is defined as the ratio of the calibration factors for absorbed dose to water at beam qualities Q and Q_0. It is expressed as [14]

$$k_{Q,Q_0} = \frac{N_{D,w,Q}}{N_{D,w,Q_0}} = \frac{D_{w,Q}/M_Q}{D_{w,Q_0}/M_{Q_0}} \quad , \tag{5}$$

where $N_{D,w,Q}$ and N_{D,w,Q_o} are the calibration factors in terms of absorbed dose to water for beam qualities Q and Q_o, $D_{w,Q}$ and D_{w,Q_o} are the absorbed doses to water for the respective beam qualities, and M_Q and M_{Q_o} are the dosimeter readings for beam qualities Q and Q_0.

In a perfect world, the beam quality correction factor should be measured directly for each chamber using the same beam quality as the clinical beam. However, most standards laboratories lack access to these specific beam qualities, so only a few specialized PSDLs can perform such measurements. Additionally, it is challenging for standards laboratories to replicate the exact beam qualities produced by clinical linacs, limiting the widespread use of this technique. When direct measurement of k_{Q,Q_o} is not feasible, or no experimental data are available for clinical beams, the correction factors can be calculated theoretically.

Using Bragg–Gray theory, an expression for k_{Q,Q_o} can be derived by comparing it with the $N_{D,air}$ formalism used in IAEA Codes of Practice (CoP) and other dosimetry protocols [20, 21]. The Bragg–Gray theory is a fundamental concept in radiation dosimetry that relates the energy deposited in a small cavity (such as an ionization chamber) to the surrounding medium. It assumes that the cavity is small enough not to disturb the charged particle fluence in the medium. The theory presumes that the small cavity (filled with gas) is embedded in a solid or liquid medium (e.g. tissue or water), and the ionization produced in the cavity is proportional to the dose absorbed in the medium. The energy deposited in the cavity comes from charged particles (e.g. electrons) generated by the surrounding medium, not by direct photon interactions in the cavity. The dose to medium is proportional to the ionization measured in the cavity, scaled by the stopping-power ratio between medium and gas.

Stopping power refers to the rate at which energy is transferred from a photon beam to the material it passes through, in this case tissue or water. However, since photons are uncharged, they do not lose energy directly as charged particles do. Instead, photons interact with matter through processes like the photoelectric effect, Compton scattering and pair production, which leads to the creation of secondary charged particles (electrons and positrons). These secondary particles are what actually deposit energy in the material.

The stopping power of the material is numerically equal to the loss of energy E per unit path length x, i.e. [22]

$$S(E) = -dE/dx \quad , \tag{6}$$

where the minus sign makes S positive. The equation above defines linear stopping power, typically expressed in units like MeV/mm, although in the International System of Units (SI, Système International d'Unités), it is measured in N. When comparing a substance in gaseous and solid states, their linear stopping powers can differ significantly due to variations in density. To account for this, the force is divided by the material's density to obtain mass stopping power (S/ρ), which is measured in units like MeV/(g/cm²) or similar, and expressed in the SI as m⁴/s². Mass stopping power is largely independent on the material density.

According to the Bragg–Grey theory, the absorbed dose is a product of electron fluence and the (average unrestricted) mass collision stopping power, and the dose ratio in air and medium can be expressed as [22]

$$\frac{D_{air}}{D_{med}} = \frac{\Phi^e_{air}\left(\frac{S}{\rho}\right)_{air}}{\Phi^e_{med}\left(\frac{S}{\rho}\right)_{med}} \quad , \tag{7}$$

where ϕ^e_{air} and ϕ^e_{med} are the electron fluence in air and medium. With the reasonable assumption that an air cavity in the medium is small enough not to perturb the secondary electron fluence in the medium, and only the charged particles crossing the air cavity deposit energy into the cavity, one can deduce the dose to medium [22]

$$D_{med} = D_{air}\left(\frac{S}{\rho}\right)^{med}_{air} \quad . \tag{8}$$

The dose to medium can therefore be expressed as a product of the dose to air and mass collision stopping-power ratio of the medium and air.

To correct for non-reference conditions, the calculation of the dose absorbed in water can be determined using the equation [23]

$$D_{w,Q} = Mk_{Tp}k_sk_{pol}k_{elec}N_{D,w,Q} \quad , \tag{9}$$

where $D_{W,Q}$ is the dose absorbed in water for radiation quality Q, M is the reading from the ionization chamber or electrometer, k_{Tp} is the temperature and pressure correction factor, k_s accounts for ion recombination due to incomplete charge collection, k_{pol} is the polarity correction factor for the ionization chamber voltage, k_{elec} adjusts for the electrometer sensitivity, and $N_{D,W,Q}$ is the ionization chamber calibration factor for radiation quality Q. The k_i influence quantities are described next.

3.1.3 Influence quantities

The calibration factor for an ionization chamber is only valid under the reference conditions used during calibration. Any deviation from these conditions when using the chamber in a different beam requires appropriate correction factors. The general correction factors are discussed in the following sections with specific factors for each type of radiation beam addressed separately.

Pressure, temperature and humidity

Since all chambers recommended by TRS-398 are open to ambient air, the mass of air in the cavity volume is affected by atmospheric variations. To convert the cavity air mass to reference conditions, the correction factor [14]

$$k_{Tp} = \frac{(273.2°C+T)}{(273.2°C+T_0)} \cdot \frac{P}{P_0} \tag{10}$$

should be applied, where P and T are the air pressure and temperature in the cavity during measurements, and P0 and T0 are the reference values (typically 101.3 kPa and 20°C). The temperature of the air in the chamber cavity should be measured and should reflect that of the phantom, which may differ from the surrounding air temperature. For measurements in a water phantom, the waterproof sleeve of the chamber should be vented to allow rapid equilibrium between the ambient air and the air in the chamber cavity [14, 23].

Electrometer calibration

When the ionization chamber and electrometer are calibrated separately, each receives its own calibration factor from the laboratory. In TRS-398, the electrometer calibration factor k_{elec} is treated as an influence quantity and included in the product $\prod k_i$ of the correction factors. Typically, the ionization chamber calibration factor $N_{D,w}$ is given in units of Gy/nC, and the electrometer calibration factor k_{elec} is either in nC/rdg (readout) or, if the electrometer measures charge, as a dimensionless factor near unity (nC/nC). If the ionization chamber and electrometer are calibrated together, the combined calibration factor $N_{D,w}$ is given in Gy/rdg or Gy/nC, depending on the electrometer readout, and no separate k_{elec} is needed. In this case, k_{elec} is recorded as unity in the worksheets [14].

Polarity effect

When commissioning an ionisation chamber, the effect of using opposite polarizing potentials must be checked. In most photon beams, the polarity effect is negligible,

except for thin window chambers used with low-energy X-rays. However, in charged-particle beams like electrons, the effect can be significant.

If a polarity effect is observed, the true reading is the average of the absolute values from both polarities. The correction factor for polarity is [14]

$$k_{pol} = \frac{|M_+| + |M_-|}{2M} \tag{11}$$

where M_+ and M_- are readings at positive and negative polarity and M is the routine reading. Readings should be stabilized after polarity changes, and it is advisable to normalize them using an external monitor. The monitor should be positioned near the chamber at the same depth.

When calibrating the chamber, the chosen polarity and potential should be used, and this must be clearly stated on the calibration certificate, including whether the polarity effect was corrected. More details of the polarity effect can be found in the TRS-398 [14].

Ion recombination

The incomplete collection of charge in an ionization chamber due to ion recombination requires a correction factor k_s. Two effects contribute: (i) general (volume) recombination, dependent on ionizing particle density and dose rate, and (ii) initial recombination, which is independent of dose rate and usually less than 0.2% for most beams. General recombination is more significant in pulsed radiation, especially in pulsed-scanned beams with high dose rates per pulse.

Boag's theory [25] can derive a correction factor, but it does not account for chamber-specific variations. A recommended approach for pulsed beams is the two-voltage method, which assumes a linear relationship between $1/M$ and $1/V$, using charge measurements M_1 and M_2 at polarizing voltages V_1 (normal) and V_2 (lower). Ideally, $V_1/V_2 \geq 3$.

The recombination correction factor k_s at the normal operating voltage V_1 is obtained from [14]

$$k_s = a_0 + a_1\left(\frac{M_1}{M_2}\right) + a_2\left(\frac{M_1}{M_2}\right)^2 \quad , \tag{12}$$

where the constants a_i are given in **Table 9** [14] for pulsed and pulsed–scanned radiation. This is valid when the chamber is homogeneously irradiated and thus applies to a point-like ionization chamber rather than an LAC. For LAC, a Jaffé plot should be used instead [24].

To minimize linac output fluctuations, all readings should be normalized to an external monitor placed near the chamber inside the phantom at a similar depth but 3-4 cm from the chamber centre.

For $k_s < 1.03$, the correction factor can be approximated to an accuracy of within 0.1% using the relation [14]

$$k_s - 1 = \frac{M_1/M_2 - 1}{V_1/V_2 - 1} \quad . \tag{13}$$

This approximation simplifies the calculation of the recombination correction factor when the recombination effect is minimal.

3.1.4 Photon beam quality specifier

The beam quality Q is specified by the $TPR_{20,10}$. This ratio compares the absorbed doses at 20 cm and 10 cm depths in a water phantom, with a source-to-detector distance (SDD) of 100 cm and a 10×10 cm^2 field size (**Figure 2**). As described earlier, the influence of electron contamination in a build-up region can be avoided, making the effective attenuation coefficient measurement more reliable. Beyond the maximum dose depth, this accurately reflects the decrease of the photon dose, which is exponential.

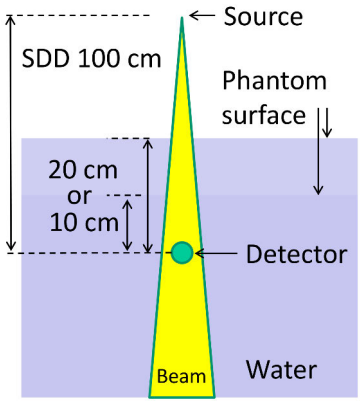

Figure 2. Schematic representation of a tissue-phantom ratio ($TPR_{20,10}$) measurement. This ratio compares the absorbed doses at 20 cm and 10 cm depths in a water phantom, with a source-to-detector distance (SDD) of 100 cm and a 10×10 cm^2 field size at the detector distance.

Because $TPR_{20,10}$ is a dose ratio, it eliminates the need for displacement correction factors used in absolute dosimetry with cylindrical chambers. Additionally, it is less affected by small positioning errors at the two depths, as both settings are impacted similarly.

There is a simple relation for $TPR_{20,10}$ [26]:

$$\mathrm{TPR}_{20,10} = 1.2661\ \mathrm{PDD}_{20,10} - 0.0595 \quad , \tag{14}$$

where $PDD_{20,10}$ is the ratio of the per cent depth doses at 20 and 10 cm depths for a field size of 10×10 cm^2 defined at the phantom surface with an SSD of 100 cm.

3.1.5 Measurements in the clinical photon beam

Before starting measurements, the stability of the dosimeter system should be checked using a reference source, allowing sufficient time for the dosimeter to reach thermal equilibrium. Some mains-powered electrometers need to be switched on at least 2 h before use for proper stabilization. It is also recommended to pre-irradiate the ionization chamber with 2-5 Gy to ensure charge equilibrium in the chamber materials. Stability is particularly crucial when modifying the polarity or polarizing voltage, as the system may take up to 20 min to stabilize, depending on the chamber and polarity. Failing to wait for stabilization can introduce errors greater than the correction being applied.

Leakage current is generated by the measuring system when no radiation is present and can increase after irradiation. It should be measured before and after irradiation and must be small, typically less than 0.1% of the measurement current. In cases like small-volume chambers at low dose rates, leakage may be higher, requiring correction based on its sign. Chambers with leakage exceeding 1% or varying over time should not be used.

When performing relative measurements in linac beams, it is highly recommended to use an additional monitoring dosimetry system to account for radiation output fluctuations. This is particularly important for measurements involving dosimeter reading ratios, such as cross-calibrations or changes in polarity or voltage. The external monitor should ideally be placed within the phantom, along the transverse plane's major axis, at the same depth as the chamber, and about 3-4 cm from the central axis. If positioned in air, temperature drifts should be considered [14].

3.1.6 Ionization chamber

An ionization chamber and a connected electrometer are used as dosimeters in the reference point dose measurements in external beam photon RT. The measurement method is based on the use of a calibrated ionization chamber. The ionization chamber measurement enables a reliable conversion of the calibration factor, based on theoretical principles, between calibration radiation quality and radiation quality used in measurements.

Cylindrical ionization chambers are used for dose measurements in high-energy photon beams of RT. The chamber volume should range between 0.1 and 1 cm^3, balancing spatial resolution with the necessary sensitivity. Typically, chambers meet

these size requirements with an inner diameter of less than 7 mm and an inner length of no more than 25 mm. The chamber wall should be as homogeneous as possible, and an air vent is required. This air opening allows the chamber to quickly stabilize to the ambient air pressure and temperature [23].

The most common chamber used for high-energy photon radiation dose measurements is the NE 2571-type Farmer ionization chamber (**Figure 3**). The traditional graphite-walled chamber is also available in a waterproof model. Chambers with graphite walls have been found to have better stability and a smoother response as a function of energy than those with plastic walls [14], while those with plastic walls are more durable.

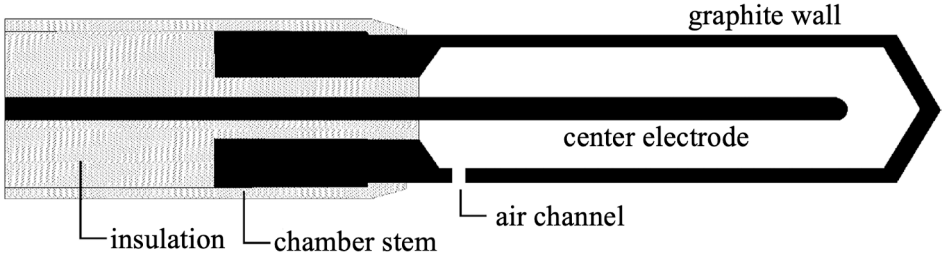

Figure 3. Structure of the Farmer-type ionization chamber used in the measurement of photon radiation (modified from [23], with permission from the Radiation and Nuclear Safety Authority of Finland).

3.1.7 Electrometer

The most reliable way to measure the small currents (of the order of picoamperes) produced by an ionization chamber is by measuring the voltage across a capacitor connected to a high-impedance operational amplifier. The measured voltage is displayed on the electrometer as charge or converted into dose units. The upper limit of the measurable charge is determined by the capacitance of the capacitor. Many electrometers and dosimeters are equipped with multiple capacitors of varying capacitance values, allowing the operating range to be divided into different measurement ranges. The selected measurement range determines which capacitor is used for the measurement [23].

Significant variations in the linearity of capacitors used across different electrometer measurement ranges have been observed, both in relation to the measured current and between the capacitors themselves. Therefore, it is essential to verify the linearity and response of the measurement ranges through testing before the device is put to use.

The electrometer typically includes an adjustable voltage source of ±500 V for setting the collection voltage of the ionization chamber. To measure the

recombination correction factor k_{rec}, the voltage must be adjustable either continuously or in steps, allowing the selection of a voltage that is 1/3 or less of the recommended collection voltage specified by the chamber manufacturer. Additionally, the voltage polarity must be reversible if the electrometer is used with chambers that require different polarities [23].

3.2 Small photon beam dosimetry

3.2.1 Small beam dosimetry standards

Small beam dosimetry is crucial for accurately measuring radiation doses in treatments like SRS, stereotactic body radiation therapy (SBRT) and other advanced techniques using narrow photon beams. As discussed earlier, small beams present unique challenges due to their size, steep dose gradients, lateral charged-particle disequilibrium and detector response limitations. There are several key dosimetry standards and protocols developed to address these challenges. In the following sections, some of the main standards available for small beam dosimetry are discussed.

IAEA TRS-483

Titled “Dosimetry of Small Static Fields Used in External Beam Radiotherapy” and published in 2017 by the IAEA [10].

TRS-483 is a widely used reference standard specifically designed to address the complexities of dosimetry in small static fields. It provides guidelines on selecting suitable detectors, performing beam data measurements and applying correction factors to account for small beam effects. TRS-483 introduces the concept of a reference field and the FOF, both being key elements for measuring small beams. It covers photon beam dosimetry for small field sizes down to 0.5 cm.

In this protocol, at least one of the following three physical conditions needs to be met for an external photon beam to be designated small:

1. there is a loss of lateral charged-particle equilibrium (LCPE) on the beam axis;
2. there is partial occlusion of the primary photon source by the collimating devices on the beam axis;
3. the size of the detector is similar or large compared with the beam dimensions.

The first two characteristics are beam-related, while the third one is detector-related for a given field size. All three conditions result in overlap between field penumbrae and detector volume.

For some treatment units it is not practical to use water phantoms for reference dosimetry, and they can be replaced by plastic phantoms mimicking the radiation interactions in water. Polymethylmethacrylate (PMMA), acrylonitrile butadiene styrene and solid water have controlled densities and defined atomic properties, allowing precise dosimeter positioning. This CoP provides a methodology for using plastic phantoms to complement dosimetry in reference conditions [10]. The main definitions and considerations in this CoP are described in the following section.

Machine-specific reference (msr) field

A machine-specific reference (msr) field is introduced for treatment units where a conventional reference field cannot be realized. The msr field should be as close as possible to the traditional reference field size and must extend at least distance r_{LCPE} beyond the outer edges of the ionization chamber. If only smaller fields are available, the msr field is typically the largest realizable field. Specific examples of msr fields for different manufacturers and linacs are outlined in Chapter 3.3 and discussed in detail in Chapter 5.3.1 of the CoP [10].

Lateral charged-particle equilibrium (LCPE) range

The parameter r_{LCPE} is crucial for determining the minimum field size and detector size where *LCPE* conditions are achieved. It depends on beam energy and was quantified by Li et al. [27] through MC calculations for various photon beam energies. The r_{LCPE} represents the smallest radius of a circular field, where the absorbed dose at the centre is related by a constant factor to the water kerma. Updated MC data express r_{LCPE} (in cm) as a function of the photon beam quality index $TPR_{20,10}$ [10]. Details of its use are provided in Chapter 5.2.1 of the CoP [10].

Volume-averaging correction factor

The volume-averaging correction factor accounts for the difference between the absorbed dose at a reference point in a water phantom and the average absorbed dose over the sensitive volume of a detector, both measured without the physical presence of the detector. It can be calculated by integrating the 3D dose distribution in the phantom over the detector volume.

For plane-parallel detectors (like ionization chambers or diodes), this can be simplified to a two-dimensional (2D) integration over the detector-sensitive area

facing the beam. For cylindrical ionization chambers, the integration requires a 2D projection of the sensitive volume, often using a weighting function for the lateral beam profile.

The equation for calculating the volume-averaging correction factor is [10]

$$k_{vol} = \frac{\iint_A w(x,y)dxdy}{\iint_A w(x,y)OAR(x,y)dx,dy} \quad , \tag{15}$$

where *x* and *y* represent the coordinates on the axes perpendicular to the beam central axis, and A denotes the area of the active volume projection. The term *OAR(x,y)* refers to the off-axis ratio or the lateral beam profile at the measurement depth, with normalization to a value of unity on the central axis. The function *w(x,y)* is a weighting factor that characterizes the extension of the ionization chamber air cavity along the beam axis.

For plane-parallel detector geometries, the weighting function *w(x,y)* remains unity across the entire integration area. Detailed examples illustrating the calculation of k_{vol} are provided in Appendix I of the CoP [10].

Beam quality

The CoP [10] suggests using beam quality data derived from specific radiation generators, as differences between treatment units of the same model are generally minimal. For reference dosimetry, these small variations mean that beam quality indices can be verified within acceptable tolerances. When such data are not available, the traditional approach of using beam quality indices must be applied. Two common indices for high-energy photon beams are $TPR_{20,10}(10)$, used in many dosimetry protocols [14], and $\%dd(10,10)_x$ [28, 29]. If a 10×10 cm^2 reference field is not achievable, the CoP recommends measuring $TPR_{20,10}(S)$ or $\%dd(10,S)_x$ for the largest square field (or equivalent square msr field for non-square fields) and then converting these to standard reference field values ($TPR_{20,10}(10)$ or $\%dd(10,10)_x$) using the formulae provided by Palmans [30].

If the SSD is not 100 cm, corrections are needed to account for inverse square law differences, electron contamination and scattering conditions. For photon beams with a flattening filter (FF), equivalent square msr fields are calculated to produce the same amount of scatter on the central axis as a rectangular or circular field. The lateral fluence distribution, approximated by the lateral beam profile, is also considered for flattening filter-free (FFF) beams.

For small fields, where traditional broad-beam methods break down due to minimal scatter, the equivalent field size is based on detector perturbation factors. In this case, the geometric mean of the length and width of a rectangular field can represent its equivalent square size. This method also extends to circular fields by

assuming equivalent areas. For fields smaller than 4 cm, phantom scatter factors are independent of collimation and linac type, depending solely on depth and field area. Hence, 4 cm is set as the transition point between broad beam field size methods and small beam techniques.

Non-traditional reference beams

Different procedures may apply to specific treatment units. For FFF beams, an additional volume-averaging correction factor may be needed due to non-homogeneous lateral beam profiles. For tomotherapy, a reference field size of 5×10 cm^2 defined at a distance of 85 cm is recommended, with a relationship established between the tomotherapy-specific beam quality index and the traditional index. The formalism by Alfonso et al. [8] is followed, advising a correction factor to reconcile differences in ionization chamber responses.

For CyberKnife systems, the largest fixed collimator-defined field is taken as a reference, typically circular with a 6 cm diameter defined at 80 cm from the source. Equivalent field and interpolation methods are used to derive beam quality indices from this field. Beam quality correction factors for ionization chambers align closely with those for other 6 MV treatment units. However, a correction greater than 1% may be necessary for long Farmer-type ionization chambers due to volume averaging.

The Gamma Knife is categorized under static small beam dosimetry, with a maximum field diameter of 1.8 cm or 1.6 cm, and reference dosimetry performed at the centre of a plastic sphere using a microchamber calibrated in a ^{60}Co gamma ray beam without a beam quality correction factor.

For Brainlab (Brainlab AG, Munich, Germany) add-ons, an SSD of 100 cm can be established, but field sizes close to 10×10 cm^2 are used instead that do not require special considerations for beam quality or reference dosimetry.

Field output factors (FOF)

An FOF is defined as the ratio of absorbed dose to water in any non-reference field to that in a reference field at a given depth. FOFs express the relationship between the absorbed dose to water in a clinical field f_{clin} and that in a reference field, either f_{msr} or f_{ref}. These factors are calculated using the ratio of detector readings, adjusted by a correction factor that converts this ratio into a ratio of absorbed dose to water. In this section, expressions are provided specifically for comparing a clinical field with a machine-specific reference field f_{msr}. However, these expressions are also applicable when comparing a clinical field with a traditional 10×10 cm^2 reference field, in which case "msr" in the equations and text is substituted with "ref."

The field output factor, $\Omega_{Q_{clin},QQ_{msr}}^{f_{clin},f_{msr}}$, [10]

$$\Omega_{Q_{clin},QQ_{msr}}^{f_{clin},f_{msr}} = \frac{M_{Q_{clin}}^{f_{clin}}}{M_{Q_{msr}}^{f_{msr}}} k_{Q_{clin},Q_{msr}}^{f_{clin},f_{msr}} \quad , \tag{16}$$

where $M_{Q_{clin}}^{f_{clin}}$ and $M_{Q_{msr}}^{f_{msr}}$ are the readings of the detector (corrected for influence quantities) in the clinical field and the msr field, respectively. Values of the output correction factor $k_{Q_{clin},Q_{msr}}^{f_{clin},f_{msr}}$ for a range of detectors are given in Tables 23 to 27 of the CoP [10].

In this thesis, an FOF for an IBA Razor™ Nano Chamber (IBA Dosimetry GmbH, Schwarzenburg, Germany) was determined and is discussed in Chapter 5.4.

Generic beam quality correction factors

In most cases, the calibration coefficient for an ionization chamber is determined in a calibration beam of quality Q_0 for a traditional 10×10 cm² reference field f_{ref}. When using this calibration coefficient in a beam with a different quality, a beam quality correction factor is necessary. The absorbed dose to water for the msr is expressed as [10]

$$D_{w,Q_{msr}}^{f_{msr}} = M_{Q_{msr}}^{f_{msr}} N_{D,w,Q_0}^{f_{ref}} k_{Q_{msr},Q_0}^{f_{msr},f_{ref}} \quad , \tag{17}$$

where $M_{Q_{msr}}^{f_{msr}}$ is the reading of the dosimeter in the msr field f_{msr} corrected for influence quantities, such as pressure, temperature, incomplete charge collection, polarity effects, etc. The term $N_{D,w,Q_0}^{f_{ref}}$ refers to the calibration coefficient for the ionization chamber in terms of absorbed dose to water. This coefficient is determined at a standards laboratory using a traditional reference calibration field f_{ref} of size 10×10 cm² with beam quality Q_0. The factor $k_{Q_{msr},Q_0}^{f_{msr},f_{ref}}$ accounts for the correction needed to address differences in the ionization chamber response when measured in the traditional reference field f_{ref} with beam quality Q_0 at the standards laboratory, versus its response in the measurement field f_{msr} with beam quality Q_{msr}.

The factor $k_{Q_{msr},Q_0}^{f_{msr},f_{ref}}$ is defined as the ratio of the ionization chamber calibration coefficients in the machine-specific and traditional reference fields [10]

$$k_{Q_{msr},Q_0}^{f_{msr},f_{ref}} = \frac{N_{D,w,Q_{msr}}^{f_{msr}}}{N_{D,w,Q_0}^{f_{ref}}} \cdot \frac{D_{w,Q_{msr}}^{f_{msr}} \Big/ M_{Q_{msr}}^{f_{msr}}}{D_{w,Q_0}^{f_{ref}} \Big/ M_{Q_0}^{f_{ref}}} , \quad (18)$$

where Q_0 typically refers to a ^{60}Co beam or a high-energy X-ray beam. In the best scenario, the correction factor would be determined by calibrating the ionization chamber in both the calibration reference field and msr field. While some standards laboratories can perform such calibrations for clinical treatment units, this service is not widely available.

It is possible to obtain more generic experimental values for beam quality correction factors using modern treatment units of the same type with similar physical characteristics. Additionally, MC calculations can provide generic beam quality correction factors for specific ionization chamber types, expressed as [10]

$$k_{Q_{msr},Q_0}^{f_{msr},f_{ref}} = \frac{D_{w,Q_{msr}}^{f_{msr}} \Big/ \bar{D}_{air,Q_{msr}}^{f_{msr}}}{D_{w,Q_0}^{f_{ref}} \Big/ \bar{D}_{air,Q_0}^{f_{ref}}} , \quad (19)$$

where all terms on the right-hand side of the equation are obtained using MC calculations. The parameter D_w corresponds to the average absorbed dose to water over a small volume surrounding the measurement point. The appropriate size of this volume depends on the dimensions of the radiation field. Similarly, D_{air} denotes the average absorbed dose to air within the cavity of the ionization chamber.

If pre-determined experimental or MC-derived beam quality correction factors are available for specific combinations of treatment units and ionization chambers, these factors are provided in Chapter 5 of the CoP [10]. Data are currently available for a limited selection of ionization chamber types and treatment machines, such as Gamma Knife, CyberKnife and tomotherapy.

It is also worth noting that calibration coefficients, such as $N_{D,w,Q_0}^{f_{msr}}$, provided by a standards laboratory may correspond to an msr field with a beam quality slightly different from the clinical msr field. In such cases, appropriate corrections are required [10]

$$D_{w,Q_{msr}}^{f_{msr}} = M_{Q_{msr}}^{f_{msr}} \, N_{D,w,Q_0}^{f_{msr}} \, k_{Q_{msr},Q_0}^{f_{msr},f_{msr}} . \quad (20)$$

No generic beam quality correction factors available

If generic beam quality correction factors for the calibration field relative to the msr field are unavailable, an alternative approach is required. In this case, the absorbed dose to water for the msr field can be calculated as follows [10]:

$$D_{w,Q_{msr}}^{f_{msr}} = M_{Q_{msr}}^{f_{msr}} N_{D,w,Q_0}^{f_{msr}} k_{Q,Q_0}^{f_{ref}} k_{Q_{msr},Q_0}^{f_{msr},f_{msr}} , \quad (21)$$

where $k_{Q,Q_0}^{f_{ref}}$ corrects for the difference between the response of the ionization chamber in a traditional calibration field f_{ref} (with beam quality Q_0) at the standards laboratory and the response of the ionization chamber in a traditional 10×10 cm^2 reference field f_{ref} (with beam quality Q) using the same machine as the msr field f_{msr}. Other parameters are as in the previous equation.

With MC calculation, it is possible to virtually establish a 10×10 cm^2 reference field and calculate the beam quality correction factor as [10]

$$k_{Q_{msr},Q}^{f_{msr},f_{ref}} = \frac{D_{w,Q_{msr}}^{f_{msr}} \Big/ \bar{D}_{air,Q_{msr}}^{f_{msr}}}{D_{w,Q}^{f_{ref}} \Big/ \bar{D}_{air,Q}^{f_{ref}}} . \quad (22)$$

In certain situations, defining the hypothetical reference field within MC calculations may necessitate adjustments not only to the secondary and tertiary collimators but also to the primary collimator, for instance with CyberKnife, which can significantly impact the beam quality.

Monte Carlo (MC) field output correction factor

The international formalism by Alfonso et al. [8] provides means to derive the MC calculated output correction factors [8]

$$k_{Q_{clin},Q_{msr}}^{f_{clin},f_{msr}} = \frac{D_{w,Q_{clin}}^{f_{clin}} \Big/ D_{det,Q_{clin}}^{f_{clin}}}{D_{w,Q_{msr}}^{f_{msr}} \Big/ D_{det,Q_{msr}}^{f_{msr}}} , \quad (23)$$

where the generic notation $D_{w,Q}$ represents the average absorbed dose to water measured within a small voxel at the reference point in a homogeneous water medium, in a radiation field of quality Q. Similarly, $D_{det,Q}$ refers to the average dose recorded in the small field detector within a field of the same quality Q.

In this thesis, a field output correction factor for an IBA Razor Nano Chamber was determined and is discussed in detail in Chapter 5.4.

AAPM TG-155

AAPM TG-155, titled "Report of AAPM Task Group 155: Megavoltage photon beam dosimetry in small fields and non-equilibrium conditions", was published in 2021 by the AAPM.

It provides comprehensive guidelines for small beam dosimetry in megavoltage (MV) photon beams. It also discusses challenges such as detector response, positioning errors and the effect of beam modifiers such as multi-leaf collimators (MLCs). The report emphasizes the importance of using appropriate detectors, such as diodes, diamond detectors and micro-ionization chambers, for small beam measurements. TG-155 also provides correction factors and methodologies for accurate dosimetry with small photon beams.

AAPM TG-51 Addendum

Titled "Addendum to the AAPM's TG-51 protocol for clinical reference dosimetry of high-energy photon beams", this was published in 2014 by the AAPM.

The TG-51 addendum extends the original TG-51 protocol to include guidance for dosimetry in small fields. It provides recommendations on the use of suitable detectors and correction factors when measuring the absorbed dose to water in small beams. While TG-51 was originally developed for broad fields, the addendum offers necessary adjustments for small beam applications.

IPEM Report 103

Titled "IPEM report 103: Small field MV photon dosimetry", this was published in 2010 by the Institute of Physics and Engineering in Medicine (IPEM).

It focuses on dosimetry techniques for small beam photon beams used in advanced RT techniques. It discusses detector choices and correction factors for accurate dose measurement in fields as small as 1 cm in diameter or less. It complements the IAEA TRS-483 in providing practical measurement techniques and calibration procedures.

AAPM TG-142

Titled "Quality Assurance of Medical Accelerators", TG-142 was published in 2009 by the AAPM.

TG-142 provides recommendations for QA in medical accelerators, with an emphasis on the use of small fields in clinical setups like IMRT and SRS. It includes guidance for beam symmetry, flatness and consistency for small beam measurements.

3.3 Dose-area product (DAP) and DAP ratio (DAPR) as a beam quality specifier

3.3.1 DAP

Traditional absolute and relative dosimetry standards in RT define dose measurements at a specific point. However, when applying point dose measurements to very small beams, potential sources of error must be addressed to ensure reliable results. These include issues such as volume averaging and the precise positioning of the point detector within the narrow beam. To mitigate these challenges, an alternative beam quality parameter for small beams has been investigated: the dose-area product ratio ($DAPR_{20,10}$). This approach involves measuring the *DAP* using a LAC. By utilizing *DAP* measurements, uncertainties related to detector positioning and volume averaging, which are common when using point detectors, are effectively eliminated (**Figure 4**).

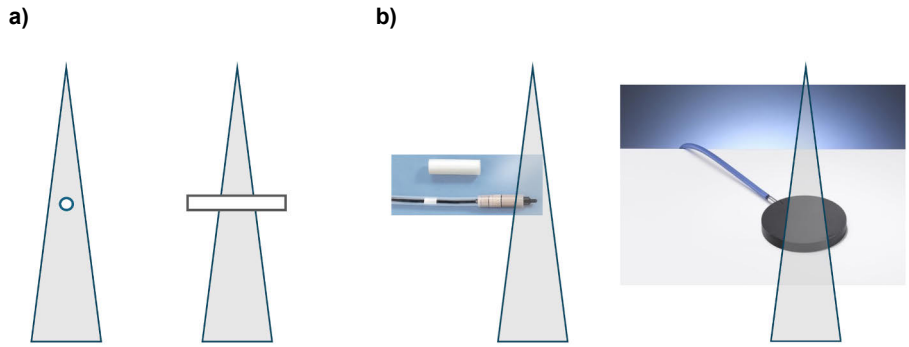

Figure 4. (**a**) Point dose (left) vs. dose-area product (DAP) (right) measurement. (**b**) Point dose detector (left) vs. large-area chamber (LAC) (right). The triangles represent conical beams (figure b modified from [31] and [32], with kind permission from PTW-Freiburg GmbH, Freiburg, Germany and IBA Dosimetry, Schwarzenbruck, Germany).

For clarity, the most common use of *DAP* is in radiography and is outlined briefly here. During radiography examinations or interventional procedures, *DAP* is used to assess the radiation exposure and resulting risk to the patient. *DAP* is determined as the absorbed dose multiplied by the area irradiated. Overall risk is better estimated

from the dose to an area than to a single point. *DAP* is measured with a *DAP* meter typically attached to the X-ray unit. In RT, and in this thesis, the *DAP* was measured in a water phantom as depicted below (**Figure 5**).

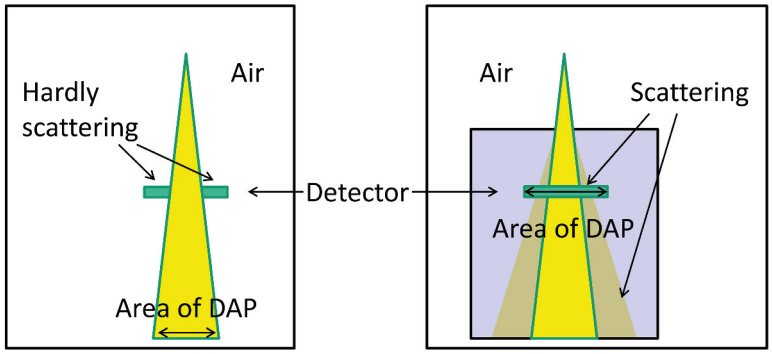

Figure 5. In diagnostic radiology (left), the dose-area product (DAP) equals the measured dose multiplied by the area of the radiation field. In small beam radiation therapy (right), *DAP* equals the measured dose multiplied by the measuring area of the detector. The yellow triangles represent conical beams and scattering.

In this work, *DAP* is defined as the absorbed dose within a specific area of interest, multiplied by that area. The area of interest is determined by the boundaries or active region of the detector. In this case, the active region corresponds to a circular area. The active area of the detector encompasses the entire beam.

*DAP*s can be derived from a 1D or 2D relative dosimeter by integrating the dose over the sensitive surface of the detector as [33]

$$DAP = 2\pi \int_0^R g(r) r dr \quad , \tag{24}$$

where R represents the radius of the integrated dose or the active volume of the detector, r denotes the off-axis distance from the beam centre, and $g(r)$ corresponds to the dose profile as a function of the distance r. This equation assumes cylindrical geometry.

In 2022, primary standards for *DAP* were established using graphite calorimetry for a broader range of small field sizes [34]. Two LACs demonstrated consistent behaviour regardless of the field shape and size. For field sizes ranging from 5 to 15 mm, the calibration coefficients exhibited slight increases with field size: 1.8% and 1.1% for the two chambers, respectively. These changes were attributed to fluence perturbation factors caused by the chamber design, as the water-to-air stopping power ratio remained constant within statistical uncertainties of approximately 0.2%, as determined by MC calculations.

A separate study showed that LACs require only minimal correction factors for DAP_w measurements and exhibit low energy dependence. Notably, the lateral setup errors of up to 5 mm are acceptable for 10×10 mm² fields, provided the beam incidence remains normal [35]. However, the limited accuracy of relative point dose measurements at the field periphery significantly restricts the overall accuracy of DAP_w measurements.

3.3.2 DAPR

The beam quality parameter, traditionally defined as the tissue-phantom ratio ($TPR_{20,10}$) at depths of 20 cm and 10 cm, has been proposed to be replaced by the dose-area product ratio ($DAPR_{20,10}$) at the same depths. This replacement is suggested for small beam RT with a fixed SSD of 100 cm [24, 33]

$$DAPR_{20,10} = \frac{DAP(d=20cm)}{DAP(d=10cm)} \quad . \tag{25}$$

Similar challenges exist for $TPR_{20,10}$ measurement as for absolute point dose measurements, including detector and beam placement uncertainty. These could be overcome by the $DAPR_{20,10}$ measurement with a LAC as illustrated below (**Figure 6**).

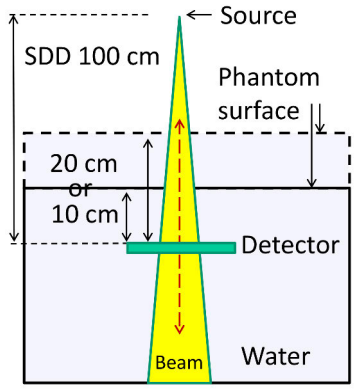

Figure 6. Dose-area product ratio ($DAPR_{20,10}$) measurement with a large-area chamber (LAC) positioned at 10 or 20 cm depths, with constant source-to-detector distance (SDD) of 100 cm. The inner surface of the entrance window of the LAC was used as the effective point of measurement.

It has been shown that the response of a PTW-type 34070 (PTW-Freiburg GmbH, Freiburg, Germany) chamber does not change with a lateral off-axis displacement of up to 2 cm in a 10×10 mm² field in water at an SSD of 100 cm [36]. This provides evidence that the positioning uncertainty is eliminated when deriving values for $DAPR_{20,10}$ compared with $TPR_{20,10}$ or PDD.

4 Materials and methods

4.1 Large-area ionization chamber (LAC)

As the name suggests, LACs are plane-parallel ionization chambers that have an ionization collection volume with a large active area. This is opposite to traditional small cylindrical volume ionization chambers for point dose measurements inside a radiation beam. They have a similar but narrower guard ring compared to plane-parallel ionization chambers used in clinical electron beam dosimetry. LACs are developed for transit dosimetry to measure the ionization generated in air by the whole beam. This data can be used in many contexts, including proton and heavy ion therapy, to monitor e.g. relative beam output deviations over time.

The LACs used in these studies are PTW Bragg Peak chambers, types 34070 (PTW.70) and 34073 (PTW.73) (PTW-Freiburg GmbH, Freiburg, Germany). These vented, waterproof, plane-parallel chambers (**Figure 7**) are designed to be connected to precision electrometers. They are used either in a water column/dry water or in a water phantom for relative measurements to determine the depth dose curve of a narrow proton or heavy ion beam of diameter of 3-10 mm.

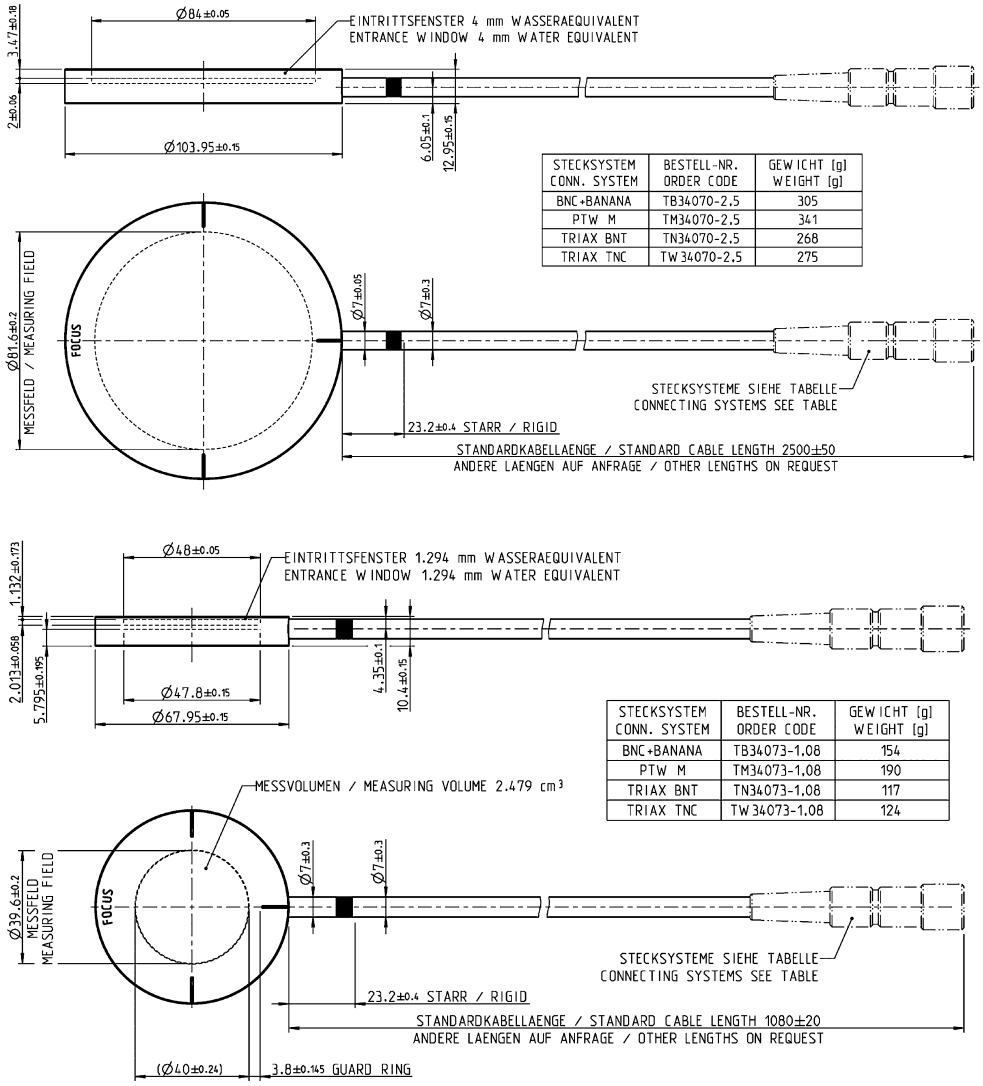

Figure 7. Construction drawings of two distinct large-area chambers (LAC). The diameters of the active volumes and the thicknesses of the entrance windows are different. PTW.70 (above) has an entrance window thickness of 3.47 mm, which corresponds to 4.00 mm of water, whereas PTW.73 (below) has an entrance window thickness of 1.13 mm, which corresponds to 1.29 mm of water (reprinted from [31], with kind permission from PTW-Freiburg GmbH, Freiburg, Germany).

Both LACs have a 2 mm thick air volume. The PTW.70 chamber, with a detector diameter of 104 mm, has a 0.10 mm lacquer entrance window, 3.35 mm PMMA and 0.02 mm graphite, corresponding to a 4.0 mm water-equivalent thickness of 6 MV photons. The air volume and the active volume diameter of this chamber are 84.0

mm and 81.6 mm, respectively. In comparison, the PTW.73 chamber has a smaller detector diameter of 68.0 mm. It has a 0.10 mm lacquer entrance window, 1.01 mm PMMA and 0.02 mm graphite, giving it a 1.29 mm water-equivalent thickness of 6 MV photons. The air volume and the active volume diameter are 48.0 mm and 39.6 mm, respectively.

To confirm that there are no manufacturing deficiencies, and that the construction drawings provided by the manufacturer are accurate, both LACs were imaged with an X-ray micro-CT device at Turku Bioscience Centre (Turku, Finland) and with an X-ray mammography unit at Turku University Hospital (Turku, Finland). Mammography and micro-CT images of the smaller LAC, PTW.73, were shown to closely replicate the construction drawings, and no manufacturing deficiencies were found (**Figure 8**).

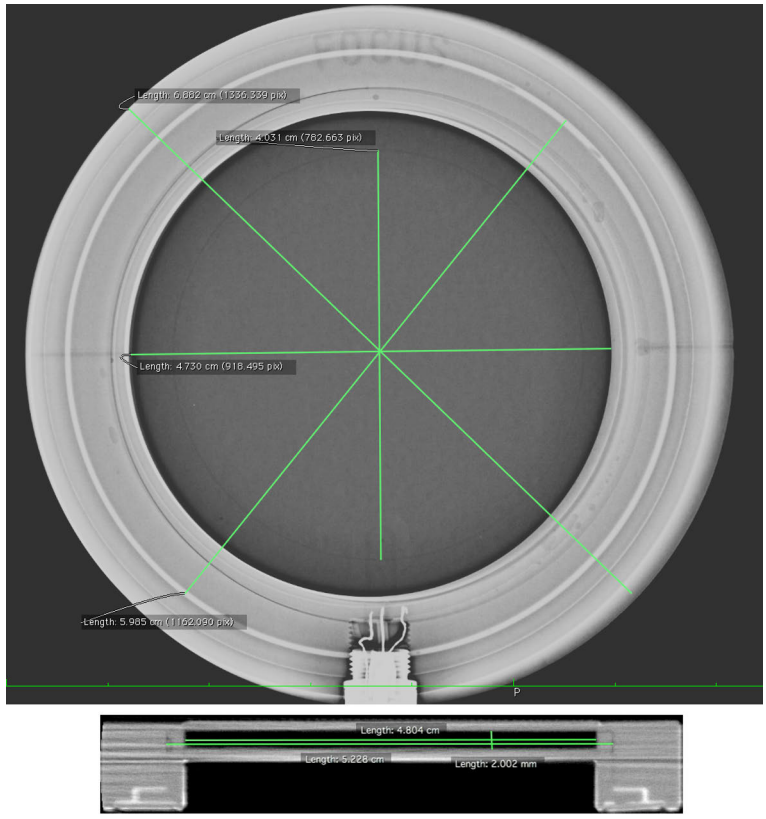

Figure 8. X-ray mammography image (upper image) and X-ray micro-CT image slice of the smaller large-area chamber (LAC) PTW.73. The measured collection electrode diameter of 40.3 mm (upper image) is close to 39.6 mm, as depicted in Figure 7 provided by the manufacturer. The measured air cavity diameter of 48.0 mm (lower image) and thickness of 2.0 mm are the same as depicted in Figure 7 provided by the manufacturer.

4.2 Radiochromic film

For relative off-axis dosimetry, Gafchromic EBT3 (Ashland Inc., Wayne, NJ, USA) radiochromic film was used in a solid water RMI phantom (Gammex RMI Inc., Middleton, WI, USA) [37]. The self-developing EBT3 film requires no additional processing [38]. Films were scanned at a resolution of 72 dots per inch (0.35 mm) with an Epson Perfection V750-M Pro (Seiko Epson Corp., Suwa, Japan) scanner, using the method by Sipilä *et al.* [39].

EBT3 film consists of a 0.030 mm thick active emulsion layer sandwiched between two identical 125 μm thick polyester substrates. These substrates are treated to embed microscopic silica particles (less than 10 μm in diameter) on their surfaces, resulting in a total film thickness of 0.280 mm. By increasing the gap between the film and the scanner glass, this treatment prevents the formation of Newton's rings, a pattern artifact that can occur when smooth surfaces, such as those of the earlier EBT2 film and flatbed scanner glass, come into close proximity at around the wavelength of the light, potentially affecting dosimetry accuracy. The silica content is minimal (less than 1%) and does not impact the EBT3 dose-response as it does with EBT2. Additionally, the symmetrical structure of the EBT3 film eliminates any potential for a side-dependent response when placed on the scanner glass [40]. The EBT3 film is used in RT dosimetry, particularly for measuring electron and mixed photon/electron dose distributions. The dosimetric accuracy of the film is influenced by several factors, including scanner sensitivity, film orientation and post-exposure changes.

The film response can be affected by the inhomogeneity of the scanner. A two-phase correction process was used in this thesis, including a matrix correction for the scanning area and a dose-dependent correction, to improve uniformity. After these corrections, the uniformity of the response can be improved to within ±50 pixel values [39].

To avoid errors, the film must be scanned in fixed orientations. Scanning in four orientations (non-rotated, rotated 180°, flipped non-rotated, and flipped and rotated 180°) and averaging the results can further improve accuracy. The film dosimetry protocol used requires that the film be read no later than 4 days after irradiation to ensure stabilization of changes in optical density.

The EBT3 film shows minimal energy dependence within 1.0% for 6 MV photon and 6-16 MeV electron beams, making it suitable for mixed beam dosimetry. The combined expanded uncertainty for absolute and relative dose measurements is approximately 3.7% (k=2) and 2.3% (k=2), respectively [39].

4.3 Point dose measurements

4.3.1 Diode detector

The IBA Razor™ Detector (IBA Dosimetry GmbH, Schwarzenburg, Germany) is an unshielded semiconductor detector based on a p-type silicon diode chip (**Figure 9**). It is designed for output factor measurements in small-to-medium-sized photon beams. Performance is assured in the range of photon beam qualities from 60Co gamma rays to 6-15 MV X-rays by the manufacturer.

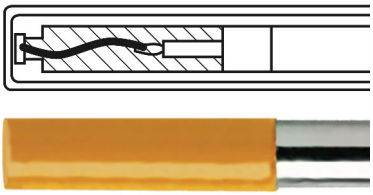

Figure 9. Schematic (above) and image (below) of the IBA Razor™ Detector with chip size 0.95 mm × 0.95 mm, thickness 0.4 mm and sensitive area of 0.6 mm (reprinted from [41], with permission from IBA Dosimetry, Schwarzenbruck, Germany).

The IBA Razor™ Detector has an active volume of diameter 0.6 mm and height 20 µm with a head diameter of 4.0 mm and total dosimeter length of 60 mm. The effective measurement point is 0.8 ± 0.2 mm from the surface. It is constructed with an n-type implant in p-type silicon and operates in photovoltaic mode requiring no bias voltage. Radiation ionization in the silicon generates electron-hole pairs, with the signal primarily produced by electrons that diffuse through the crystal to the n-p junction region, where they are swept up by the built-in electric field of the depleted region. Electron pairs generated directly within the depleted region contribute minimally to the signal [42].

4.3.2 Diamond detector

The PTW microDiamond (PTW-Freiburg GmbH, Freiburg, Germany) is a synthetic diamond detector. Unlike silicon diode detectors, this type of detector is highly resistant to radiation damage. The active measurement area is 4 mm^2 and the active volume 0.004 mm^3, with volume thickness 0.001 mm. It exhibits minimal energy and dose-rate dependence and can measure fields up to 400×400 mm^2 in size.

4.3.3 Medium size ionisation chamber

The PTW Semiflex 31010 (0.125 cm^3) (PTW-Freiburg GmbH, Freiburg, Germany) used in this thesis is a point ionization chamber with an active volume of 0.125 cm^2. It is a suitable compromise between small size for reasonable spatial resolution and large sensitive volume for precise dose measurements. It also has a small directional response. The sensitive volume is nearly spherical with a diameter of 5.5 mm. The reference point is 4.5 mm from the detector tip. It can be used with field sizes from 30×30 mm^2 to 400×400 mm^2.

4.3.4 Small size ionisation chamber

The IBA Razor™ Nano Chamber (IBA Dosimetry, Schwarzenbruck, Germany) is an air-filled microchamber with outer and inner electrodes made of Shonka (C-552) plastic and graphite, respectively [43]. The active volume is 3 mm^3 and the diameter of the active volume is 2 mm (**Figure 10**). It is intended for small beam output factors, depth dose curve and *OAR* measurements. Its strength as an ionization chamber is that it does not exhibit oversensitivity to scattered low-energy photons as is the case with unshielded diodes. With a small active volume, however, the noise starts to play a role in the measurements, necessitating longer measurement times.

In this thesis, the FOFs and field output correction factors have been determined for this chamber.

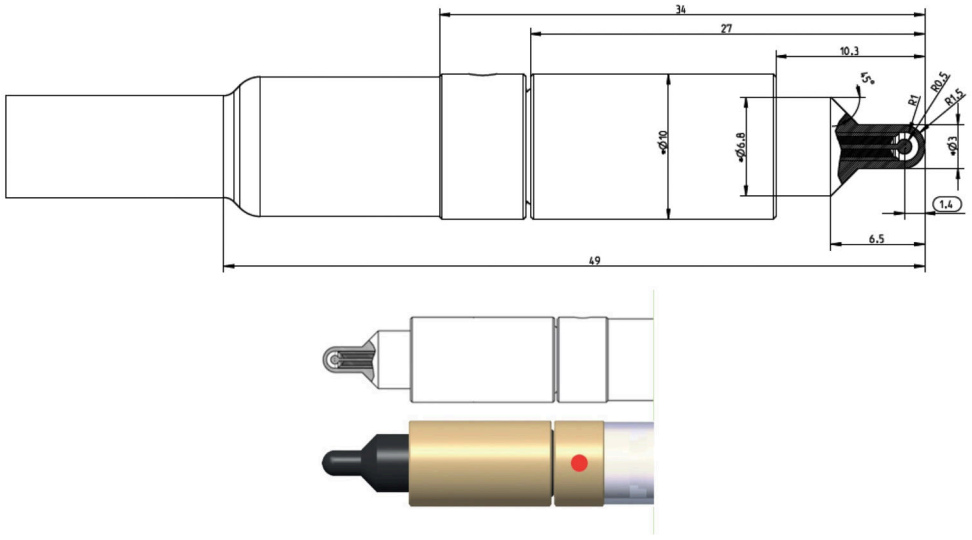

Figure 10. Construction drawing and image of the IBA Razor™ Nano Chamber (reprinted from [32, 41], with kind permission from IBA Dosimetry, Schwarzenbruck, Germany).

4.4 Off-axis ratio (OAR), dose-area product (DAP) and *DAP* ratio (DAPR) determination

4.4.1 *DAP* and *DAPR* determination with LAC

The dose-area product ratio at 20 and 10 cm depths ($DAPR_{20,10}$) with a constant SSD of 100 cm can be measured as shown below (**Figure 11**) versus a traditional $TPR_{20,10}$ beam quality specifier.

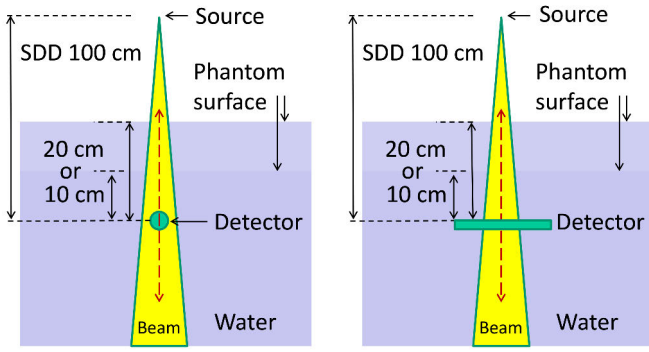

Figure 11. Measurement of the tissue-phantom ratio ($TPR_{20,10}$) with a traditional point dose detector (left), and of the dose-area product ratio ($DAPR_{20,10}$) with a large-area chamber (LAC) (right). Both measurements were done with a constant source-to-detector distance (SDD) of 100 cm.

When placing the detector in water, special care must be taken due to the hollow bottom of the larger PTW.70 chamber. Careless immersion can cause air bubbles to form under the active volume of the detector, potentially affecting the *DAP* measurement results. Although this effect largely cancels out in *DAPR* measurements, a sizeable effect cannot be ruled out. Therefore, to prevent air bubbles, it is good practice to immerse the detector upside down and only then turn it right side up while it remains submerged.

Measurements were done in the following sequence:

- Connect the electrometer and switch it on.
- Perform all necessary adjustments to the electrometer.
- Verify that any high voltage is correctly adjusted.
- Connect the detector.
- Allow for a stabilization time of 15 min before starting the measurement.

- Pre-irradiate the detector.
- Check the leakage current, which should be low and stable.
- Perform a zero adjustment.
- Perform the measurement.

While the nominal bias voltage is +400 V for the PTW.70 and PTW.73 chambers, in this thesis, a smaller and opposite polarity voltage of -250 V was used to mitigate the polarity effect.

4.4.2 *OAR* and *DAP* determination with radiochromic film

In this thesis, as described in Study I, EBT3 film was employed within a solid water phantom to measure the *OAR* and determine the *DAP* for various field sizes. Solid water was chosen due to challenges of accurately positioning a film in water at the required depths and the risk of water infiltrating between the film layers, which can affect the readout. Four films were irradiated at two different dose levels to optimize the dose response both within and outside the beam. Specifically, two 10×20 cm² films were exposed to 2 Gy to evaluate the beam profile, ranging from a 100% dose at the centre to 50% in the penumbra region. The remaining two films were irradiated with dose levels ranging from 4 Gy to 20 Gy at the centre, enabling the assessment of beam profiles beyond the 50% dose level. This approach improved the accuracy of low-dose region profile evaluations, with calibration remaining valid up to 10 Gy. Finally, *OAR* and *DAP* measurements were compared with MC calculations and IBA Razor diode measurements to evaluate the feasibility of $DAPR_{20,10}$ determination using radiochromic film.

4.4.3 *OAR*, *DAP* and *DAPR* determination with a point dose detector

In Study I, the IBA Razor diode detector was used for direct *PDD*, *OAR* and $TPR_{20,10}$ measurements, as well as for the subsequent $DAPR_{20,10}$ determination. The beam axis and the detector axis were positioned vertically in all measurements, with the detector pointing upwards.

The *OAR*s in both lateral and longitudinal directions were averaged, and the resulting dose integral for *DAP* determination was calculated and compared with the results of film measurements and MC calculations.

Furthermore, following the *OAR* measurements at depths of 10 cm and 20 cm, and performing the corresponding *OAR* integration to derive *DAP(d=20cm)* and *DAP(d=10cm)*, $DAPR_{20,10}$ was calculated according to Eq. (24) using an integration radius corresponding to the active area of the LAC chamber, as described in Study I.

In Study II, central axis profiles and *PDD*s obtained with the IBA Razor Nano Chamber were compared with those from recommended small beam detectors, including the IBA Razor diode and PTW microDiamond detectors. Additionally, the traditional PTW Semiflex (0.125 cm³) detector was used for larger field sizes. The full width at half maximum (FWHM) and the penumbrae (defined as the distance between the 80% and 20% dose points) were determined using the Profeel dosimetry data analysis and visualization software described in [44].

4.5 Study of small photon beams

Measurements were conducted at Tampere University Hospital (Tampere, Finland) and Turku University Hospital (Turku, Finland) using a variety of beam shapes and sizes. These included conical collimators (CC) (Brainlab AG, Munich, Germany) with diameters ranging from 4 mm to 40 mm, square jaw-defined beams sized between 10 mm and 200 mm, square MLC-shaped beams ranging from 5 mm to 20 mm, and additional MLC-shaped beams measuring 10×10 mm², as illustrated below (**Figure 12**).

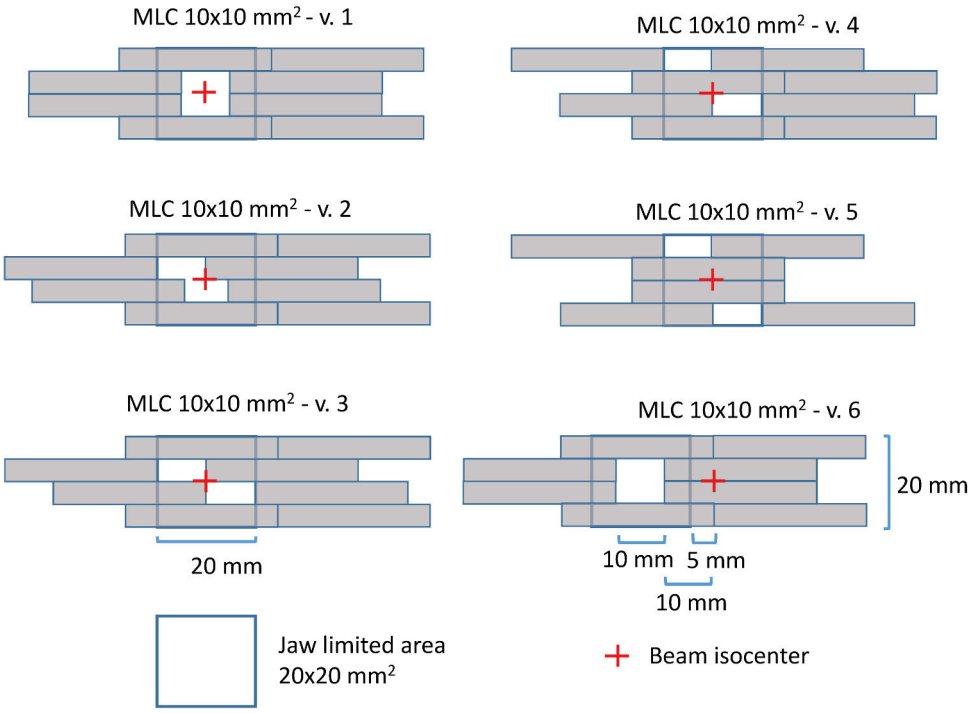

Figure 12. Diagrams of six multi-leaf collimator (MLC) -shaped fields, where the width of a leaf is 5 mm (modified from Study III and reproduced by permission of IOP Publishing. All rights reserved © 2021 IOP Publishing Ltd).

Measurements were performed using three medical linacs: one Varian Clinac iX and two Varian TrueBeam systems (Varian Medical Systems, Inc., Palo Alto, CA, USA). The studied beams included traditional FF beams with nominal energies of 6 MV and 18 MV, as well as FFF beams with nominal energies of 6 MV and 10 MV.

4.6 Monte Carlo (MC) calculations for large-area ionisation chambers

To verify the $DAPR_{20,10}$ measurement results obtained from the various detectors, MC calculations were employed to derive the same metrics. Additionally, the perturbations caused by air cavities and the detector's physical material were investigated in the *DAPR* measurement.

In this thesis, four types of MC calculations were studied: 1) air-to-water $DAPR_{20,10}$ ratio ($DAPR_{20,10,air}/DAPR_{20,10,w}$), 2) detector-to-water $DAPR_{20,10}$ ratio ($DAPR_{20,10,det}/DAPR_{20,10,w}$), 3) $DAPR_{20,10}(r)$ in water and 4) $DAPR_{20,10}$ for each LAC, fully simulated detectors in water. These geometries are shown in **Figure 13**. *DAP*s from MC calculations were derived from the absorbed dose in the specified water or air volume in a water slab, air slab in water, or air slab in the detector. For dose-to-water simulations, these volumes were concentric water rings around the central water cylinder. For dose-to-air simulations in water or in the detector, they were single air cylinder slabs.

The Monte Carlo (MC) calculations were carried out using the EGSnrc software system (Electron Gamma Shower, National Research Council, Ottawa, ON, Canada), versions 2016 and 2017 [45]. The geometry of the Varian Clinac iX was modelled using the BEAMnrc user code, which is part of the EGSnrc system [46-49]. The Varian TrueBeam MC model utilized phase-space (phsp) files provided by the manufacturer, recorded at a plane above the jaws, which were subsequently used as sources for BEAMnrc treatment head simulations. The input file for the remaining treatment head geometry included the jaws, an approximate model of the collimator baseplate, the multi-leaf collimator (MLC) in a parked position, the light field reticle, and the interface mount, with all geometrical and material properties provided by the manufacturer. The CCs with diameters of 4-5 mm were modelled based on manufacturer specifications, and their dimensions were verified through measurements. The phsp files generated from the linac beam models were then used as particle sources for dose calculations in the phantom using the egs_chamber user code.

To evaluate $DAPR_{20,10}(r)$, the dose-area product ratio as a function of the integrated dose radius r in water, dose profiles were scored in 0.2 mm thick water slabs for beam diameters of 0.2 mm, 7.5 mm and 15 mm, at depths of 10 cm and 20 cm, with SSDs of 90 cm and 80 cm, respectively. For the 7.5 mm CC beam, a ring

thickness of 2.00 mm was applied across the full profile, with finer ring widths used for specific regions: 0.25 mm inside the beam, 0.50 mm up to the 10% *OAR*, 1.00 mm up to 30.00 mm off-axis, and 2.00 mm up to 100.00 mm. All rings were centred on the beam central axis. The collected data were used to evaluate the suitability of the IBA Razor diode for profile measurements in water, and film measurements in solid water, for *DAP* assessments. Further details regarding the EGSnrc transport parameters can be found in Studies I and III.

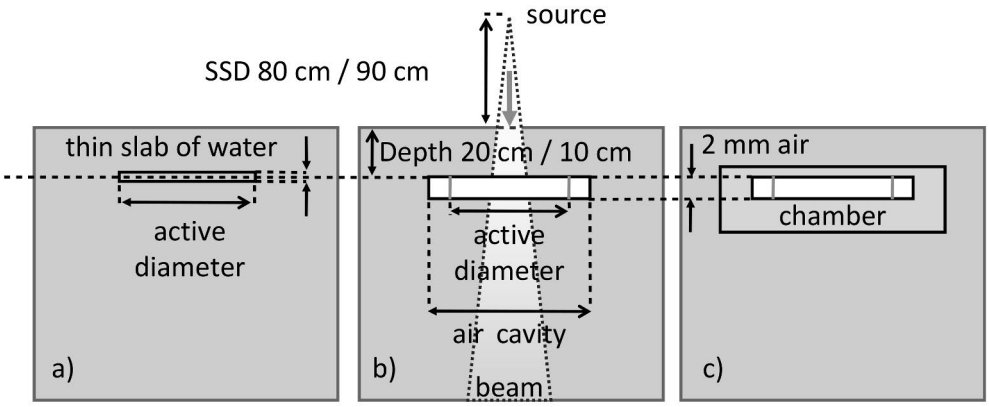

Figure 13. The MC calculations were performed to simulate geometries for scoring the integral dose in volumes corresponding to the active volumes of PTW.73 or PTW.70 chambers and in thin water slabs. Grey represents water and white represents air. The incident beam is illustrated only in (b). In (a), the dose was scored in a thin 0.2 mm thick water slab with diameters matching the active volumes of 39.6 mm or 81.6 mm. The centre of the water slab volume was located at a depth of 10 cm with an SSD of 90 cm, and at a depth of 20 cm with an SSD of 80 cm. In (b), the air volumes corresponded to the LAC air volumes, with a thickness of 2.0 mm and diameters of 48.0 mm or 84.0 mm, respectively. Scoring volumes matched the active or measuring volumes of the LACs, with diameters of 39.6 mm or 81.6 mm. The entrance surface of the air volume was positioned at depths of 10 cm or 20 cm in water. In (c), the complete LACs were modelled, including the front and back wall electrodes and guard rings. The entrance surface of the air volume was again positioned at depths of 10 cm or 20 cm in water. (MC = Monte Carlo; LAC = large-area chamber; SSD = source-to-surface distance) (modified from Study I and reproduced by permission of IOP Publishing. All rights reserved © 2021 IOP Publishing Ltd).

For simulated parallel beams, a spectrum derived from a jaw-collimated 10×10 mm² FF beam from a Varian TrueBeam linac was used. The phsp file was recorded below the jaws at a distance of 45 cm from the target level. The photon energy spectrum was determined using BEAMDP software, part of the EGSnrc system, within an area of 7×7 mm² to form the parallel beam energy spectrum, as illustrated below (**Figure 14**). This area encompasses the full jaw opening with an additional margin of 1.25 mm on all sides. The recorded spectrum closely approximates

realistic small beam spectra generated by the linacs used in this study. As shown (**Figure 14**), the photon energy fluence passing through the jaws is roughly 3-5% of the photon energy fluence outside the jaws for photon energies ranging between 0.5 MeV and 5 MeV, respectively. The electron kinetic energy fluence contributes less than 0.1% of the in-field energy fluence. The simulated parallel beams, originating from a plane located 45 cm from the source, were transported through air slabs with thicknesses of 35 cm and 45 cm for SSDs of 80 cm and 90 cm, respectively, before reaching the water phantom.

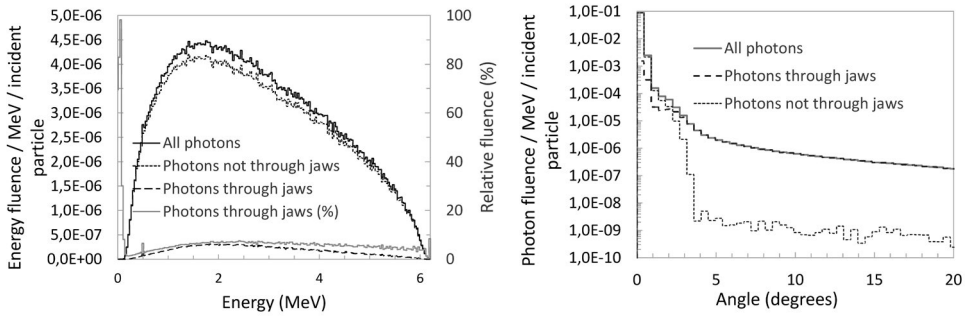

Figure 14. The energy spectra fluences (left) and the angular distribution of photon fluence (right) were recorded within a 7×7 mm² area of a 10×10 mm² field (at 100 cm from the target). The scoring was performed just below the jaws at a distance of 45 cm from the target (modified from Study III and reproduced by permission of IOP Publishing. All rights reserved © 2021 IOP Publishing Ltd).

4.7 Monte Carlo (MC) calculations for IBA Razor Nano Chamber

In this thesis, the field output correction factors $k_{Q_{clin},Q_{msr}}^{f_{clin},f_{msr}}$ and field output factors $\Omega_{Q_{clin},Q_{msr}}^{f_{clin},f_{msr}}$ were determined according to the TRS-483 protocol. The machine-specific reference field size of 10×10 cm^2 and clinical field sizes of 0.5×0.5, 1×1, 2×2 and 3×3 cm^2 were simulated.

MC calculations were conducted using EGSnrc [45]. Photon beams with nominal energies of 6 MV, 6 MV FFF and 10 MV FFF from the TrueBeam linac were modelled using the BEAMnrc user code [50] at an SSD of 100 cm, with phsp files provided by Varian. The IBA Razor Nano Chamber was modelled according to manufacturer blueprints using the egs_chamber user code [51]. The chamber model was used for profile and *PDD* simulations, as well as for field output correction factor and FOF simulations. All simulations were conducted in a large cylindrical water phantom with a 30 cm radius and 40 cm height, using the recommended material files [52].

5 Summary of the Results

Three of the original publications (I-III) included in this thesis deal with novel dosimetry methods for small photon fields in external beam RT. The main aspects of the work lay in the development of dose measurement methods. New chamber types and a beam quality specifier were studied with measurements and supporting MC calculations.

A novel beam quality specifier, $DAPR_{20,10}$, was studied to assess its feasibility in characterizing beam quality in small beams. This involved examining how the properties of the small beams and large chambers influence the measurement quantities *DAP* and $DAPR_{20,10}$. Multiple detector types were compared with each other for deriving these metrics. The potential practical and clinical applications of this novel method for small RT beams is discussed.

FOFs and field output correction factors were determined for a new small ionization chamber, the IBA Razor Nano Chamber. These correction factors represent novel findings for this chamber and the studied beams. Additionally, the applicability of the IBA Razor Nano Chamber for small beam *PDD* and *OAR* measurements was investigated by comparing its results against those achieved with other established small-volume detectors. The feasibility of a novel method for beam quality measurement is explored in Studies I and III, and a new small ionization chamber for small beam measurements is examined in Study II.

5.1 *DAPR* determined with LAC, film, point dosimeter and MC calculations

Measurements with 6 MV FF beams showed a constant $DAPR_{20,10}$ value for fields 20-40 mm in diameter with a maximum relative change of 0.6%, whereas there was a 7.0% increase for fields of 4-20 mm in diameter with the PTW Type 34070 chamber (**Table 1**). In Study I, a small error was identified in the results. The error is small, with maximum value of 0.87%, affecting only four tabulated results in **Table 1** of the study. The error is in the MC-calculated $DAPR_{20,10}$ ratio for one chamber, because the reported results were not updated after a re-simulation with a slightly enhanced chamber model prior to publication. **Table 1** now includes the corrected values. The revised results show that the difference between the MC

calculation and measurements is actually smaller, dropping from 2.1% to 1.2%. This correction does not affect any conclusions in the paper regarding the validity and applicability of the methods; on the contrary, results improved slightly after correction. The maximum difference between the MC-calculated $DAPR_{20,10}$ values and measurements was 1.2%. On average, the *DAP* ratios were 1.1% greater for 7.5-30 mm CCs and 0.4% greater for the 4 mm CC compared to measurements. For PTW.70, the calculations agreed with measurements showing a maximum deviation of 0.2% for 10-40 mm CCs. For the 4 mm and 7.5 mm CCs, the differences were –1.2% and –1.0%, respectively.

Table 1. Measured and calculated dose-area product ratio ($DAPR_{20,10}$) and their relative difference for the two large-area chambers (LAC), PTW.73 and PTW.70, for a 6 MV beam with a flattening filter. Overall, the calculated dose-area product (DAP) ratios agree with measurements showing a maximum relative difference of –1.2%. One standard deviation is shown in parentheses (modified from Study I and reproduced by permission of IOP Publishing.).

		Cone collimator diameter (mm)					
Chamber	**Type**	**4**	**7.5**	**10**	**20**	**30**	**40**
PTW.73	Meas.	0.656(7)	0.635(8)	0.632(7)	0.626(7)	0.626(7)	-
PTW.73	MC	0.658(1)	0.641(1)	0.639(1)	0.633(0)	0.633(0)	-
MC to meas.	Diff. (%)	0.41	0.95	1.16	1.18	1.10	-
PTW.70	Meas.	0.702(5)	0.674(5)	0.663(5)	0.655(5)	0.651(5)	0.651(5)
PTW.70	MC	0.693(1)	0.667(1)	0.661(0)	0.654(0)	0.652(0)	0.651(0)
MC to meas.	Diff. (%)	-1.24	-1.04	-0.19	-0.11	0.18	0.02

Both simulations and measurements indicated that $DAPR_{20,10}$ increases with larger LAC size or dose integration area for the 4-40 mm CC-collimated 6 MV photon beams (**Figure 15a**). Consequently, it is important to specify the active area of the LAC or the *DAP* integration area when reporting $DAPR_{20,10}$ values.

To evaluate the variations of $DAPR_{20,10}$ with beam size and shape, MC-calculated $DAPR_{20,10}$ values in water were analysed as a function of the integrated dose radius for four distinct beams, as shown below (**Figure 15b**). The beams included a 0.2 mm diameter parallel beam (PB0.2mm), 7.5 mm diameter parallel beam (PB7.5mm), 15 mm diameter parallel beam (PB15mm) and a fully simulated, CC-collimated 7.5 mm diameter beam with FF and corresponding beam divergence (CC7.5mm) with a jaw setting of 50x50 mm^2. The overall mean and maximum relative statistical uncertainties of the scored voxel doses used to calculate the $DAPR_{20,10}$ values (**Figure 15b**) were 0.1%, 0.9%, 0.1%, 3.2%, 0.1%, 3.9%, 0.1% and 0.3%, respectively.

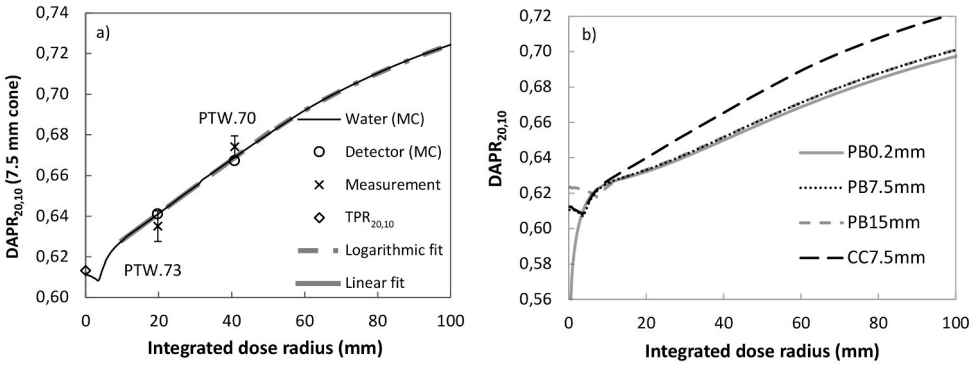

Figure 15. The $DAPR_{20,10}$ is shown as a function of the integrated dose radius for a 7.5 mm cone collimator (a) and a parallel beam with varying diameters (b), including 0.2 mm (PB0.2mm), 7.5 mm (PB7.5mm), and 15 mm (PB15mm). For comparison, a 7.5 mm cone-collimated beam with a flattening filter (CC7.5mm) is also included, using a jaw opening of 50 mm. MC-calculated $DAPR_{20,10}$ values were obtained in water and within the active volume of the detector. The results are represented as solid lines for water and circles for detector volumes, while LAC measurements are marked with crosses, including the associated measurement errors (1σ). The statistical uncertainty in the MC-calculated ratios was approximately 0.001, which is smaller than the displayed symbols. For $DAPR_{20,10}$ in water, the data were modelled using a linear fit from 10 to 50 mm and a logarithmic fit from 50 to 100 mm. Additionally, the measured $TPR_{20,10}$ value, obtained with the IBA Razor diode, is included for comparison, providing a reference point within the overall analysis. ($DAPR_{20,10}$ = dose-area product ratio at 20 and 10 cm depth; $TPR_{20,10}$ = tissue-phantom ratio at 20 and 10 cm depth; MC = Monte Carlo; LAC = large-area chamber; OAR = off-axis ratio; SSD = source-to-surface distance; CAX = centre-of-axis; MC = Monte Carlo, PB = parallel beam, CC = conical collimator) (modified from Studies I and III and reproduced by permission of IOP Publishing. All rights reserved © 2021 IOP Publishing Ltd).

The feasibility of circular beam $DAPR_{20,10}$ measurements with other detectors was investigated by determining the *DAP* using point detector off-axis measurements in water and film measurements in a solid water phantom. The study was conducted with a 7.5 mm cone and a 6 MV FF beam. The off-axis profiles for the 7.5 mm cone, measured with the IBA Razor diode and EBT3 film, are shown alongside MC calculations (**Figure 16a, 16b**). Additionally, Farmer ionization chamber measurements at two out-of-field points, marked with crosses, were included (**Figure 16b**). The *DAP* was integrated from these normalized profiles, where 100% corresponds to the CAX, following the method described in Eq. (24). The integrated *DAP* values are presented below (**Figure 16c**).

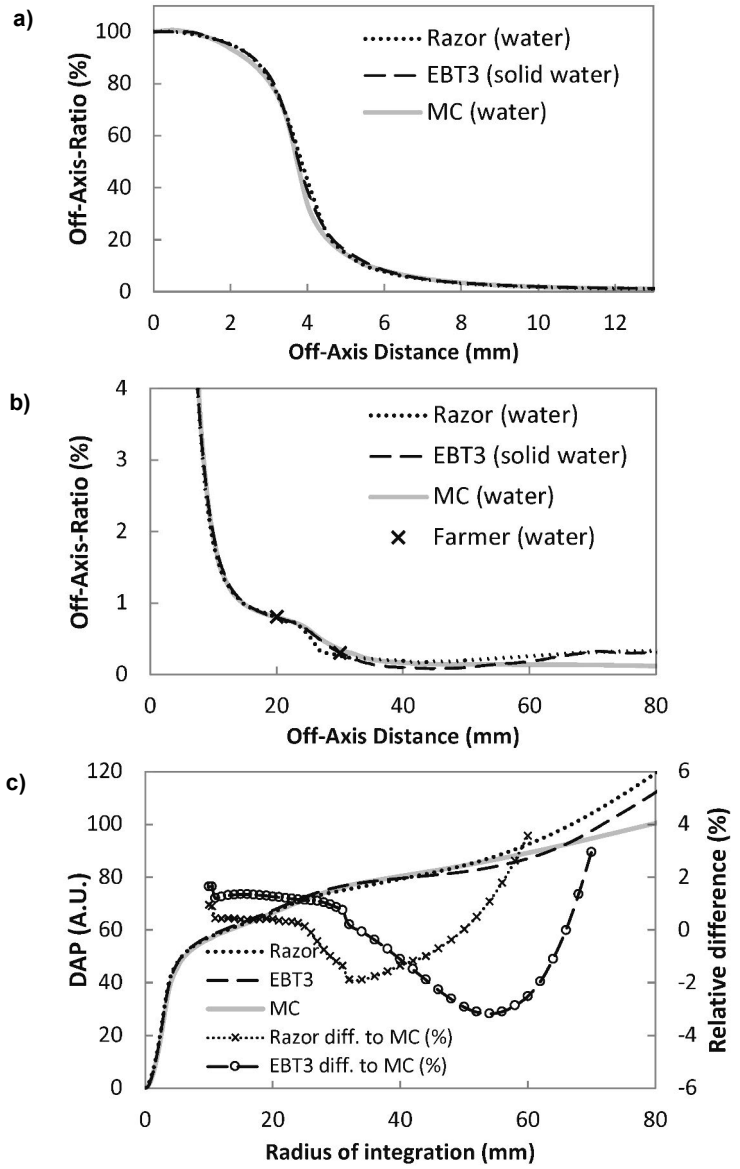

Figure 16. Measured and calculated central-axis normalised profiles for the 7.5-mm diameter cone collimator at a depth of 10 cm and an SSD of 90 cm (a and b). Measurements with the IBA Razor diode and Farmer ionization chamber were performed in water, while EBT3 film measurements were conducted in solid water. MC calculations were also performed in water for comparison. The *DAP* was integrated from the profiles (a and b) using data from the IBA Razor diode, EBT3 film measurements and MC calculations. The figure shows the resulting integrated *DAP* values (c) (MC = Monte Carlo; DAP = dose-area product; A.U. = arbitrary unit; SSD = source-to-surface distance) (modified from Study I and reproduced by permission of IOP Publishing. All rights reserved © 2021 IOP Publishing Ltd).

5.2 *DAPR* with functions of photon beam size, energy and shape

This work showed that $DAPR_{20,10}$ increases with beam energy similarly to $TPR_{20,10}$ but, contrary to $TPR_{20,10}$, it had only a minimal dependency on beam size and shape. The $DAPR_{20,10}$ indices measured with two LACs for three linacs, four beam energy types and various field sizes and shapes are presented in **Table 2**.

Table 2. Measured dose-area product ratio ($DAPR_{20,10}$) indices for PTW34073 and PTW34070 LACs (LAC = large-area ionization chamber, linac = linear accelerator, FS = jaw-defined field size, Cone = diameter of conical collimator, MLC = multi-leaf collimator, FF = flattening filter, FFF = flattening filter-free, TB = TrueBeam) (modified from Study III and reproduced by permission of IOP Publishing. All rights reserved © 2021 IOP Publishing Ltd).

				PTW34073				PTW34070			
				Beam type (nominal energy and flattening filter)							
Linac	**FS (mm)**	**Cone (mm)**	**MLC (mm)**	**6 MV FF**	**18 MV FF**	**6 MV FFF**	**10 MV FFF**	**6 MV FF**	**18 MV FF**	**6 MV FFF**	**10 MV FFF**
Clinic2 iX	50	4	-	0.656	0.751	-	-	0.702	0.777	-	-
Clinic2 iX	50	7.5	-	0.635	0.746	-	-	0.674	0.774	-	-
Clinic2 iX	50	10	-	0.632	0.745	-	-	0.663	0.769	-	-
Clinic2 iX	50	20	-	0.626	0.745	-	-	0.655	0.770	-	-
Clinic2 iX	50	30	-	0.626	0.756	-	-	0.651	0.770	-	-
Clinic2 iX	50	40	-	-	-	-	-	0.651	0.770	-	-
Clinic2 TB	20	4	-	-	-	0.606	0.677	-	-	-	-
Clinic2 TB	20	7.5	-	-	-	0.596	0.674	-	-	-	-
Clinic2 TB	20	10	-	-	-	0.597	0.671	-	-	-	-
Clinic2 TB	20	15	-	-	-	0.593	0.673	-	-	-	-
Clinic1 TB	10	-	-	-	-	-	-	-	-	0.625	0.697
Clinic1 TB	20	4	-	-	-	0.603	-	-	-	0.635	0.705
Clinic1 TB	20	7.5	-	-	-	0.597	-	-	-	0.622	0.697
Clinic1 TB	20	10	-	-	-	0.596	-	-	-	0.620	0.696
Clinic1 TB	20	15	-	-	-	0.594	-	-	-	0.617	0.694
Clinic1 TB	20	-	5	0.640	-	0.619	-	0.663	-	0.644	-
Clinic1 TB	20	-	10	0.629	-	0.605	-	0.657	-	0.627	-
Clinic1 TB	20	-	15	0.625	-	0.598	-	0.652	-	0.622	-
Clinic1 TB	20	-	20	0.624	-	0.594	-	0.647	-	0.611	-
Clinic1 TB	20	-	-	0.626	-	0.593	-	-	-	-	0.688
Clinic1 TB	20	-	10v2	-	-	0.603	-	-	-	0.625	-
Clinic1 TB	20	-	10v3	-	-	0.600	-	-	-	0.626	-
Clinic1 TB	20	-	10v4	-	-	0.600	-	-	-	0.620	-
Clinic1 TB	20	-	10v5	-	-	0.601	-	-	-	0.620	-
Clinic1 TB	20	-	10v6	-	-	0.601	-	-	-	0.625	-
Clinic1 TB	30	-	-	0.629	-	-	-	-	-	-	-
Clinic1 TB	50	4	-	-	-	0.625	-	-	-	0.671	0.724
Clinic1 TB	50	7.5	-	-	-	0.605	-	-	-	0.638	0.707
Clinic1 TB	50	10	-	-	-	0.600	-	-	-	0.630	0.702
Clinic1 TB	50	15	-	-	-	0.596	-	-	-	0.622	0.698
Clinic1 TB	50	-	-	0.633	-	0.601	-	-	-	0.619	0.690
Clinic1 TB	100	-	-	0.658	-	0.625	-	-	-	0.628	0.701
Clinic1 TB	200	-	-	-	-	-	-	-	-	0.664	0.728

5.3 Perturbations in *DAPR* determination

Small differences were observed between $DAPR_{20,10}$ evaluated in an air volume and in a water volume, with a maximum difference of 0.6% as shown in **Table 3**. Similarly, MC calculations showed a maximum difference of 0.8% between detector and water evaluations of $DAPR_{20,10}$. The overall average and maximum relative statistical uncertainties of the scored voxel doses to calculate $DAPR_{20,10}$ values were 0.08% and 0.17%, respectively.

Table 3. Monte Carlo (MC)-calculated dose-area product ratios ($DAPR_{20,10}$) of "air to water" and "detector to water" (modified from I and reproduced by permission of IOP Publishing. All rights reserved © 2021 IOP Publishing Ltd).

		Cone collimator diameter (mm)						
Ratio	**Chamber**	**4**	**7.5**	**10**	**20**	**30**	**40**	**Avg.**
$DAPR_{(20,10),air}$/	PTW.73	1.006	1.001	1.002	1.001	1.000	1.005	1.003
$DAPR_{(20,10),w}$	PTW.70	1.006	0.999	1.001	1.000	1.000	1.000	1.001
$DAPR_{(20,10)det}$/	PTW.73	1.006	0.999	1.003	1.001	1.002	-	1.002
$DAPR_{(20,10),w}$	PTW.70	1.008	0.998	1.000	1.000	0.999	1.000	1.001

5.4 Properties of a new small cavity ionization chamber in small photon beams

Study II characterized the properties of the small cavity ionization chamber, the IBA Razor Nano Chamber, through comparative dose measurements with other detectors and MC calculations. FWHM and penumbra (80%-20%) beam parameters for the 6 MV inline profiles at the central axis are presented in **Table 4**. Additionally, the $TPR_{20,10}$ was derived from the *PDD*s following the CoP described in [14] for the Nano Chamber, microDiamond and Semiflex detectors, using a 10×10 cm² field size. The $TPR_{20,10}$ values obtained with the Nano Chamber were found to be 0.48, 1.80 and 0.87% smaller than with the microDiamond, and 1.24, 1.79 and 1.17% smaller compared with the Semiflex, for the 6 MV, 6 MV FFF and 10 MV FFF beams, respectively. The maximum differences were observed with the 6 MV FFF beam.

Table 4. Full-width at half maximum (FWHM) and penumbra (80%-20%) values for measured inline profiles at the central axis for a 6 MV flattening filter (FF) beam at a depth of 5 cm (modified from Study II and reproduced by permission of IOP Publishing. All rights reserved © 2021 IOP Publishing Ltd).

Field size (mm^2)	FWHM (mm)				Penumbra (mm)			
	IBA Nano Chamber	IBA Razor Diode	PTW micro-Diamond	PTW Semi-flex	IBA Nano Chamber	IBA Razor Diode	PTW micro-Diamond	PTW Semi-flex
10x10	10.3	10.2	-	-	3.5	3.0	-	-
20x20	19.5	20.7	-	-	3.0	3.4	-	-
30x30	30.3	3.03	31.1	31.3	3.2	3.2	3.8	5.5
100x100	104.1	-	104.7	105.3	3.8	-	4.4	6.3
400x400	420.7	-	421.9	422.1	5.4	-	8.1	7.5

The determined correction factors $k_{Q_{clin},Q_{msr}}^{f_{clin},f_{msr}}$ are novel findings for the IBA Razor Nano Chamber in photon beams from the Varian TrueBeam. The $TPR_{20,10}$ values obtained with the IBA Razor Nano Chamber were 0.5, 1.8 and 0.9% smaller than with the microDiamond and 1.2, 1.8 and 1.2% smaller than with the Semiflex in studied beam energies of 6 MV, 6 MV FFF and 10 MV FFF, respectively. The maximum differences were observed with the 6 MV FFF beam. The determined FOFs from MC calculations and measurements, as well as the field output correction factors from MC calculations, are listed in **Tables 5** and **6**.

Table 5. Field output factors (FOF) determined with Monte Carlo (MC) calculations and measurements for beam energies of 6 MV and 10 MV with flattening filter (FF) and flattening filter free (FFF) beams (modified from Study II and reproduced by permission of IOP Publishing. All rights reserved © 2021 IOP Publishing Ltd).

	6 MV FF			6 MV FFF			10 MV FFF		
f_{clin} (mm^2)	MC	Meas-ured	Diff. (%)	MC	Meas-ured	Diff. (%)	MC	Meas-ured	Diff. (%)
5×5	0.457	0.479	-4.8	0.505	0.502	0.6	0.403	0.453	-12.4
10×10	0.729	0.740	-1.5	0.762	0.761	0.1	0.701	0.743	-6.0
20×20	0.842	0.831	1.3	0.866	0.849	1.9	0.867	0.877	-1.2
30×30	0.876	0.859	1.9	0.896	0.874	2.5	0.912	0.916	-0.4

Table 6. Field output correction factors determined with Monte Carlo (MC) calculations for beam energies of 6 MV and 10 MV with flattening filter (FF) and flattening filter free (FFF) beams (modified from Study II and reproduced by permission of IOP Publishing. All rights reserved © 2021 IOP Publishing Ltd).

f_{clin} (mm^2)	6 MV FF	6 MV FFF	10 MV FFF
5x5	1.028	1.034	1.036
10x10	0.996	1.002	1.008
20x20	0.992	1.001	1.001
30x30	0.988	0.992	0.996

6 Discussion

In Studies I and III, the aim was to evaluate a novel beam quality specifier, $DAPR_{20,10}$, as an alternative to the established traditional beam quality specifier $TPR_{20,10}$ for small photon fields in external beam RT. While $TPR_{20,10}$ works well in traditional larger beams, it faces challenges in small beams due to the placement uncertainty within the small beam. $TPR_{20,10}$ also increases with field size [30, 53]. However, the $DAPR_{20,10}$ exhibits greatly reduced field size dependence compared with the $TPR_{20,10}$ and has been reported to be wholly independent of field size [24, 33, 54].

Similar studies have been conducted to measure the DAP and determine a calibration factor [24, 34, 55]. FOFs have been determined with *DAP* [55, 56] in solid water. Additionally, the beam quality parameter $TPR_{20,10}$ has been proposed to be replaced by $DAPR_{20,}$10 with a constant SSD of 100 cm in small beam RT [33].

In Study I, MC calculations and measurements of $DAPR_{20,10}$ in water revealed a small dependence of the LAC size for CC-collimated 6 MV beams. The $DAPR_{20,10}$ remains mainly constant with field size, with a minor exception in the smallest CC-collimated fields. Comparisons with another study [24] show agreement for larger fields but deviations for smaller CCs, possibly attributed to differences in LAC design and beam collimation. For CC-shaped field diameters of 7.5, 10 and 20 mm, the authors [24] found relatively constant $DAPR_{20,10}$ values of 0.645, 0.644 and 0.644 with a 6 MV beam from a Saturn 43 linac, respectively. These values are intermediate to the results from this study, as shown in **Table 1**. The LAC used in the referenced study had a diameter of 3 cm, which is smaller than both LACs used in our study. As a result, the $DAPR_{20,10}$ value measured with a 3 cm diameter LAC for the 7.5-mm CC beam and the linac in this study would be expected to be less than 0.635 according to the PTW.73 measurement, and roughly equal to 0.635 based on the water calculation (**Figure 15a**). This 1.4% deviation (0.635 vs. 0.644) may be due to differences in beam quality, as well as variations in beam collimation and LAC construction.

$DAPR_{20,10}$ has been shown to increase with integration area beyond the field FWHM due to greater contributions from scattered low-energy photons at 20 cm depth.

In Study III, it was demonstrated that for FF beams and CCs with diameters ranging from 4 mm to 30 mm and a jaw opening of 50 mm, the average $DAPR_{20,10}$ values for the 6 MV beam were 0.635 ± 0.011 for the PTW.73 chamber and 0.669 ± 0.018 for the PTW.70 chamber. For the 18 MV beam, the corresponding values were 0.749 ± 0.004 for PTW.73 and 0.772 ± 0.003 for PTW.70. The results indicate that the variation in the $DAPR_{20,10}$ index is notably smaller for the 18 MV FF beam with CC collimation compared to the 6 MV beam for both chambers. These results confirm that $DAPR_{20,10}$ is indeed constant with field size, whereas deviations are induced with increasing beam profiles relative to the *OAR* maximum beyond the FWHM by e.g. scatter radiation from the treatment head, as shown in **Figure 5**.

The increase in $DAPR_{20,10}$ with a larger integration area can be attributed to the greater contribution of low-energy scattered photons at a water depth of 20 cm compared to 10 cm. This contribution ratio rises as the radius of the dose integral increases, as illustrated (**Figure 3b**) in Study I. It was shown in Study III that the mechanism and geometry of the beam-limiting devices have a significant impact on the $DAPR_{20,10}$ values. This is evident in **Figure 15b**, where the MC-calculated *DAPR* values for CC-collimated beams are higher than those for parallel beams. Additionally, the *DAPR*s have been observed to approach the typical values of $TPR_{20,10}$ for these beams as the integrated dose radius approaches 0 mm. This aligns with the definition of $TPR_{20,10}$, which represents the ratio of the dose at 20 cm and 10 cm depths at a point. Beam penumbrae are also visible in **Figure 16b** at integrated dose radii of 3.75 mm and 7.5 mm for the 7.5 mm and 15 mm diameter beams, respectively. In addition, **Table 1** shows that for increased jaw opening from 20 to 50 mm, the $DAPR_{20,10}$ increases to a constant CC diameter.

A moderate variation in $DAPR_{20,10}$ values is observed with changes in field shape and intensity, as shown in **Table 1**. The extent of this variation also depends on the LAC used. The largest relative change, 1.2%, was observed with the larger LAC for the 4 and 5 field shape configurations. The overall standard deviations of 0.3% for PTW.73 and 0.5% for PTW.70 indicate that the changes in $DAPR_{20,10}$ are moderate when the field shape and intensity vary.

For MC-calculated parallel beams without treatment head collimation, ranging from 0.2 to 15 mm in diameter, the $DAPR_{20,10}$ index remains constant at 0.633 ± 0.001 for the PTW.73 chamber and at 0.652 ± 0.001 for the PTW.70 chamber. This demonstrates that the beam size has a minimal effect on the index when the beam energy is kept constant.

As the $DAPR_{20,10}$ values depend not only on the beam properties but also on the integration area or size of LAC used, any reported $DAPR_{20,10}$ value should specify the size of the LAC active area or the dose integration area.

Study I clearly shows that the relative out-of-field contribution to *DAP* is higher for CCs smaller than 20 mm compared with larger ones. Consequently, both *DAP*

values and the *DAP* ratio increase more rapidly with increasing integration area for smaller CCs. This effect is likely driven primarily by increased collimator scatter but may also be influenced by factors such as source occlusion, lateral electron disequilibrium and radiation leakage from the linac head.

The small differences in $DAPR_{20,10}$ between dose to air and water volumes and dose to detector and water volumes (**Table 3**), with a maximum relative difference of 0.6% and 0.8%, respectively, indicate that the air volume or detector in water has minimal impact on $DAPR_{20,10}$ compared with the water volume doses evaluated by MC calculations. The perturbations in these media effectively cancel out in measurements of the ratio of *DAP*s.

LACs show potential in small beam dosimetry for beam quality measurements, reducing uncertainties in positioning and small-volume dosimeter effects, ultimately enabling faster and more accurate measurements.

In Study II, the results show that the IBA Razor Nano Chamber is a high-resolution detector, making it suitable for small beam profile measurements down to field sizes of 20×20 mm² and for *PDD* measurements. It demonstrates the smallest FWHM and penumbra values for all field sizes except for 10×10 mm² (**Table 4**). For this field size, the IBA Razor Diode shows FWHM and penumbra values that are 0.1 mm and 0.5 mm smaller, respectively. This observation aligns with other findings [57], which reported that the IBA Razor Nano Chamber penumbra was, on average, 0.6 mm larger than that of the IBA Razor Diode and 0.5 mm larger than that of the microDiamond. This difference is attributed to the larger volume effect of the ionization chamber compared to that of the solid-state detectors. However, the reported overestimation observed in the out-of-field region (i.e. doses less than a few percent of the dose on the beam axis) [57] was only noted for the smallest field size (10×10 mm²) in this thesis. The small active volume of the Razor Nano Chamber makes it a high-resolution detector, suitable for small beam profile measurements down to field sizes of 20×20 mm².

The field output correction factors $k_{Q_{clin},Q_{msr}}^{f_{clin},f_{msr}}$ and field output factors $\Omega_{Q_{clin},QQ_{msr}}^{f_{clin},f_{msr}}$ were determined according to the TRS-483 protocol. In the 6 MV and 10 MV FF and FFF beams, the correction factors $k_{Q_{clin},Q_{msr}}^{f_{clin},f_{msr}}$ were within 1.2% for the largest field sizes, whereas correction factors as high as 3.6% were observed for the smallest field size of 5×5 mm^2 (**Table 6**). Correction factors close to unity suggest that the Razor Nano Chamber is a reliable detector for small beam output factor measurements. This conclusion aligns with earlier observations [58], where similar correction factors were reported for photon beams from the Gamma Knife Perfexion.

As shown in **Table 5**, FOFs determined via MC calculations and experimental methods revealed significant differences in small fields (5×5 mm²), likely due primarily to uncertainties in detector positioning and jaw alignment. To minimize

these systematic uncertainties, multiple setups and repeated measurements are recommended during small beam dosimetry.

For 6 MV FF and FFF beams, experimental FOFs were generally smaller than MC-calculated values, while for the 10 MV FFF beam, experimental FOFs exceeded the MC ones. These discrepancies may stem from the notable polarity effect of the IBA Razor Nano Chamber. Previous studies reported polarity correction factors of 1.009 [59] for 6 MV FF beam and up to 1.05 [58] for 6 MV and 10 MV FF beams. Applying a 1.009 polarity correction [59] for 6 MV FF and FFF beams, the experimental and MC-calculated FOFs align within 2%, which is an acceptable deviation. However, polarity correction factors for the 10 MV FFF beam remain unreported, and if similar to those of 10 MV FF beam [59], they could further increase the deviations.

The 10 MV FFF beam results require additional validation, including both detector and linac MC model verification and considerations of polarity and volume averaging effects, especially for the smallest fields of less than 10×10 mm² in size.

7 Conclusions and future aspects

In this thesis, a new beam quality specifier, the dose-area product ratio $DAPR_{20,10}$, was evaluated along with multiple detectors and their properties in the context of small beam dosimetry for external RT.

$DAPR_{20,10}$ was shown to be largely constant with respect to field size and shape, unlike the traditional $TPR_{20,10}$ reported in earlier literature. However, deviations were observed for certain small beam types, particularly those with elevated *OAR* resulting from an extended amount of scattered radiation from the treatment head. $DAPR_{20,10}$ increases with increasing energy, as does the $TPR_{20,10}$.

For circular beams, $DAPR_{20,10}$ can be determined with LACs and point and film dosimeters. For non-circular fields, this is impractical and a LAC is the only feasible option, as it measures the *DAP* of the whole beam at the same time.

The $DAPR_{20,10}$ value has proven to be a feasible beam quality parameter, with a measurement setup comparable to that of the $TPR_{20,10}$ parameter. By utilizing the known size of the LAC, this method offers the potential to enhance the accuracy of beam quality determination by reducing uncertainties related to detector placement. Consequently, the improved precision in beam quality measurements is expected to lead to increased accuracy in determining the absorbed dose in patients, particularly when employing small photon beams in external beam RT.

The clinical significance of adopting $DAPR_{20,10}$ in place of $TPR_{20,10}$ for small beam RT should be thoroughly assessed by evaluating the overall uncertainty in the calculated patient target dose when using $DAPR_{20,10}$ compared with $TPR_{20,10}$ as a beam quality metric. Further research, including additional simulations and experimental data on LAC response curves and perturbation factors, is needed to identify the optimal LAC characteristics. This will ensure accurate traceability of the absorbed dose and *DAPR* from beams in a standards laboratory to the user beams in a clinical environment, across varying beam dimensions and energy levels, ultimately establishing a robust $DAPR_{20,10}$-based beam quality specifier.

New FOFs and field output correction factors were determined for a small cavity ionization chamber through comprehensive measurements and MC calculations. In addition, *PDD* and *OAR* profile measurements were compared with well-established small beam detectors. The IBA Razor Nano Chamber MC model was validated using

OAR and *PDD* simulations, where the dose deposition was calculated within the active volume of the complete detector model. The simulation outcomes were compared with measured data through dose difference and distance-to-agreement analyses. These comparisons indicate that the IBA Razor Nano Chamber MC model aligns well with the experimental measurement results. In conclusion, the IBA Razor Nano Chamber was shown to be suitable for small beam dosimetry including *PDD* and *OAR* measurements, as well as for FOF measurements.

Acknowledgements

I would like to express my heartfelt gratitude to my supervisor, Associate Professor Jani Keyriläinen, for his unwavering support throughout my studies and the writing of this thesis. Without his support, this task would have been impossible! I extent my sincere thanks to my supervisor, Associate Professor Jarkko Ojala, for his invaluable guidance and support. Our discussions on the Monte Carlo calculation design were always deeply engaging and instrumental in constructing appropriate models. It has been a wonderful experience to work with such professionals.

I am also most grateful to the reviewers, Professor Sauli Savolainen and PhD Stephane Dufreneix, for their time and effort in reviewing this thesis. Their invaluable feedback made this dissertation so much better. I would also like to thank my opponent, Conjoint and Adjunct Professor Joerg Lehmann, for travelling from the other side of the world to participate in my defence and for helping me to finalise the entire process. Many thanks to my Custos, Professor Petriina Paturi, for her unwavering guidance through my studies and the thesis-writing process.

I also wish to thank my co-authors, Mari Partanen and Petri Sipilä, who spent many weekends at the Turku and Tampere clinics conducting measurements, and to Mari for designing, constructing and simulating the Monte Carlo calculations. Thank you to Mikko Björkqvist for support on the first paper. I also deeply appreciate the continuous support of Associate Professor Mika Kapanen throughout these years.

There are many close friends to whom I wish to express my gratitude for always believing in my ability to complete this work. I am particularly grateful to my musician friends for offering a fresh perspective on life and helping me to enjoy the moment. These include, in no particular order, Jissant, Talambo, Niño, Seija, Schtimbo, Bama, Rentu, Emmi, Rumppasrömmi, Pete and Thimbu. They taught me, in the end, what music truly is.

I owe immeasurable gratitude to my loving family. My parents, grandparents and sister have always supported my endeavours. They encouraged me to pursue my passions, opening the doors to a variety of experiences, whether being a government official, a professional musician, a hospital worker in cancer care, an entrepreneur building tools for cancer treatment, and who knows what next.

Finally, I extend from the bottom of my heart my deepest thanks to my loving wife and my two dear sons for their immeasurable support and understanding during these busy times. Balancing the demands of running a company, completing this thesis and pursuing my studies over the past few years has not always been easy. Yet your support, trust and belief in me never faltered. Thank you Rahel, Dominic and Alex! I love you!

February 11th, 2025
Jarkko Niemelä

List of References

[1] Kapanen M, Sipilä P, Bly R, Järvinen H, Tenhunen M, "Accuracy of central axis dose calculations for photon external radiotherapy beams in Finland: the quality of local beam data and the use of averaged data.", *Radiother Oncol.* 86(2): 264-71, 2008.

[2] Kapanen M, Tenhunen M, Hämäläinen T, Sipilä P, Parkkinen R, Järvinen H, "Analysis of quality control data of eight modern radiotherapy linear accelerators: the short- and long-term behaviours of the outputs and the reproducibility of quality control measurements.", *Phys Med Biol.* 51(14):3581-92, 2006.

[3] Capote R, Sánchez-Doblado F, Leal A, Lagares JI, Arráns R, Hartmann GH, "An EGSnrc Monte Carlo study of the microionisation chamber for reference dosimetry of narrow irregular IMRT beamlets", *Med Phys.* 31(9):2416-22, 2004.

[4] Low DA, Moran JM, Dempsey JF, Dong L, Oldham M, "Dosimetry tools and techniques for IMRT", *Med Phys.* 38(3):1313-38, 2011.

[5] Dawson LA, Jaffray DA, "Advances in Image-Guided Radiation Therapy", *J Clin Oncol.* 10;25(8):938-46, 2007.

[6] Pappas E, Maris TG, Manolopoulos S, Zacharopoulou F, Papadakis A, Green S and Wojnecki C, "Stereotactic radiosurgery photon field profile dosimetry using conventional dosimeters and polymer gel dosimetry. Analysis and inter-comparison", *Journal of Physics*: Conference Series 164, 2009.

[7] Indra Das J, George Ding X and Ahnesjö A, "Small fields: Nonequilibrium radiation dosimetry", *Med Phys.* 35(1):206-15, 2008

[8] Alfonso R, Andreo P, Capote R, Huq MS, Kilby W, Kjäll P, Mackie TR, Palmans H, Rosser K, Seuntjens J, Ullrich W, Vatnitsky S, "A new formalism for reference dosimetry of small and nonstandard fields", *Med. Phys.* 35(11):5179-5186, 2008.

[9] Castro P, García-Vicente F, Mínguez C, Floriano A, Sevillano D, Pérez L, and Torres JJ, "Study of the uncertainty in the determination of the absorbed dose to water during external beam radiotherapy calibration", *Journal of Appl. Clin. Med. Phys.*, 9(1), 2008.

[10] International Atomic Energy Agency (IAEA) "Dosimetry of small static fields used in external beam radiotherapy. An international code of practice for reference and relative dose determination." Sponsored by the IAEA and AAPM. *Technical Report Series 483*. Vienna: IAEA; 2017.

[11] Sauer OA and Wilbert J, "Measurement of output factors for small photon beams", *Med. Phys.* 34:1983–1988, 2007.

[12] Seuntjens J and Verhaegen F, "Comments on 'Ionisation chamber dosimetry of small photon fields: A Monte Carlo study on stopping-power ratios for radiosurgery and IMRT beams'," Phys. Med. Biol. 48, L43–45, 2003.

[13] Technical document: "Brainlab Novalis Conical Collimators" 4167x-xx 60911-80.

[14] International Atomic Energy Agency (IAEA) "Absorbed Dose Determination in External Beam Radiotherapy. An International Code of Practice for Dosimetry Based on Standards of Absorbed Dose to Water." *Technical Report Series 398 (Rev. 1)*. Vienna: IAEA; 2024.

[15] Ahnesjö A, Weber L and Nilsson P. “Modeling transmission and scatter for photon beam attenuators” *Med. Phys.* 22:1711–20, 1995.

[16] Marttila O, “Suureet ja yksiköt,” *Säteily ja sen havaitseminen*, T. K. Ikäheimonen, Ed. Hämeenlinna: Säteilyturvakeskus, pp. 66–91, 2002.

[17] Hohlfeld K “The standard DIN 6800: Procedures for absorbed dose determination in radiology by the ionisation method”, *Dosimetry in Radiotherapy* (Proc. Symp. Vienna, 1987), 1:13–22, Vienna: IAEA: 1988

[18] Andreo P “Absorbed dose beam quality factors for the dosimetry of high-energy photon beams”, *Phys. Med. Biol.* 37:2189–2211, 1992.

[19] Rogers DWO “The advantages of absorbed-dose calibration factors” *Med. Phys.* 19:1227–1239, 1992.

[20] International Atomic Energy Agency (IAEA) “Absorbed dose determination in photon and electron beams. An international code of practice” *Technical Report Series No. 277*, Vienna: IAEA; 1987.

[21] International Atomic Energy Agency (IAEA) “The Use of Plane-parallel Ionisation Chambers in High-energy Electron and Photon Beams. An International Code of Practice for Dosimetry” *Technical Reports Series No. 381*, Vienna: IAEA, 1997.

[22] Podgorsak EB, International Atomic Energy Agency (IAEA) “Radiation Oncology Physics: A Handbook for Teachers and Students”, STI/PUB/1196, July 2005.

[23] Kosunen A, Sipilä P, Parkkinen P, Jokelainen I, Järvinen H. “Sädehoidon annosmiattukset - Ulkoisen sädehoidon suurenergisten fotoni- ja elektronisäteilykeilojen kalibrointi” *STUK-STO-TR 1 Technical Report*, February 2005.

[24] Dufreneix S, Ostrowsky A, Le Roy M, Sommier L, Gouriou J, Delaunay F, Rapp B, Daures J and Bordy J-M “Using a dose-area product for absolute measurements in small fields: a feasibility study” *Phys. Med. Biol.* 61:650–662, 2016.

[25] Boag JW “Ionisation measurements at very high intensities. I. Pulsed radiation beams”, *Brit. J. Radiol.* 23:601, 1950.

[26] Followill DS, Tailor RC, Tello VM, and Hanson WF “An empirical relationship for determining photon beam quality in TG-21 from a ratio of percent depth doses” *Med. Phys.* 25:1202–1205, 1998.

[27] Li XA, Soubra M, Szanto J, and Gerig LH “Lateral electron equilibrium and electron contamination in measurements of head-scatter factors using miniphantoms and brass caps” *Med. Phys.* 22:1167–1170, 1995.

[28] Almond PR et al. “AAPM’s TG-51 protocol for clinical reference dosimetry of high-energy photon and electron beams” *Med. Phys.* 26:1847–1870, 1999.

[29] McEwen M. et al. “Addendum to the AAPM’s TG-51 protocol for clinical reference dosimetry of high-energy photon beams” *Med. Phys.* 41:041501-1–20, 2014.

[30] Palmans H, “Determination of the beam quality index of high-energy photon beams under nonstandard reference conditions,” *Med. Phys.* 39:5513–5519, 2012.

[31] User Manual: “PTW Bragg Peak Chamber 34070 and 34073”; Bragg_Peak_chamb_34070-73_Man_en_79713100_06.

[32] Brochure: IBA Dosimetry, “DETECTORS For Relative and Absolute Dosimetry Ionization Chambers and Diode Detectors”; Detectors-RD-_-AD_Rev.3_0718_E.

[33] Pimpinella M, Caporali C, Guerra AS, Silvi L, De Coste V, Petrucci A, Delaunay F, Dufreneix S, Gouriou J, Ostrowsky A, Rapp 4B Bordy J-M, Daures J, Le Roy M, Sommier L, Vermesse D “Feasibility of using a dose-area product ratio as beam quality specifier for photon beams with small field sizes” *Phys Med.* 45:106-116, 2018.

[34] Jurczak J, Rapp B, Delaunay F, Gouriou J, Dufreneix S, Bordy J-M "Dose-area product primary standards established by graphite calorimetry at the LNE-LNHB for small radiation fields in radiotherapy" *Physica Medica* 98:18-27, 2022.

[35] Kupfer T, Lehmann J, Butler DJ, Ramanathan G, Bailey TE, Franich RD "Commissioning of a PTW 34070 large-area plane-parallel ionisation chamber for small field megavoltage photon dosimetry" *J. Appl. Clin. Med. Phys.* 18(6):206-207, 2017.

[36] Sánchez-Doblado F, Hartmann G H, Pena J, Roselló J V, Russiello G, Gonzalez-Castaño D M "A new method for output factor determination in MLC shaped narrow beams" *Phys. Med.* 23:58–66, 2007.

[37] Tello V M, Taylor R C and Hanson W F "How water equivalent are water-equivalent solid materials for output calibration of photon and electron beams?" *Med. Phys.* 22(7):1177-89, 1995.

[38] Dreindl R, Georg D, and Stock M "Radiochromic film dosimetry: Considerations on precision and accuracy for EBT2 and EBT3 type films" *Z. Med. Phys.* 24:153–163, 2014.

[39] Sipilä P, Ojala J, Kaijaluoto S, Jokelainen I, Kosunen A "Gafchromic EBT3 film dosimetry in electron beams — energy dependence and improved film read-out" *J. Appl. Clin. Med. Phys.* 17(1):5970, 2016.

[40] Lewis D, Micke A, Yu X, Chan MF. "An efficient protocol for radiochromic film dosimetry combining calibration and measurement in a single scan." *Med Phys.* 39(10):6339–50, 2012.

[41] Technical document: IBA Dosimetry, "Razor Nano Chamber User's Guide"; P-16-010-510-001 02.

[42] Reggiori G, Mancosu P, Scorsetti M et al. "Characterization of a new unshielded diode for small field dosimetry under flattening filter free beams" *Physica Medica* 32(2):408-413, 2016.

[43] Reggiori G, Stravato A, Mancosu P, et al. "Small field characterization of a Nanochamber prototype under flattening filter free photon beams." *Phys. Med.* 49:139-146, 2018.

[44] Pakarinen, T, Ojala, J "Profeel - An Open Source Dosimetry Data Visualization and Analysis Software." *Comput Methods Programs Biomed*, 212, p. 106457, 2021.

[45] Kawrakow I, Mainegra-Hing E, Rogers D W O, Tessier F, Walters B R B "The EGSnrc Code System: Monte Carlo Simulation of Electron and Photon Transport" *Report PIRS-701,* National Research Council of Canada. Ottawa, Canada, 2016.

[46] Ojala J, Hyödynmaa S, Pitkänen M "BEAMnrc Monte Carlo modelling of linear accelerator using parallel computing grid – validation of a common, fixed geometry model for photon and electron beams." *Proceedings of XVIth ICCR*, Amsterdam, Netherlands, pp 1-4, 2010.

[47] Ojala J, Hyödynmaa S, Baran´czyk R, Góra E, Waligórski MP "Performance of two commercial electron beam algorithms over regions close to the lung–mediastinum interface, against Monte Carlo simulation and point dosimetry in virtual and anthropomorphic phantoms" *Phys Med.* 30:147–54, 2014.

[48] Ojala JJ, Kapanen MK, Hyödynmaa SJ, Wigren TK, Pitkänen MA "Performance of dose calculation algorithms from three generations in lung SBRT: comparison with full Monte Carlo-based dose distributions" *J. Appl. Clin. Med. Phys.* 15(2):4662, 2014.

[49] Ojala J, Kapanen M, Sipilä P, Hyödynmaa S, Pitkänen M "The accuracy of Acuros XB algorithm for radiation beams traversing a metallic hip implant – comparison with measurements and Monte Carlo calculations" *J. Appl. Clin. Med. Phys.* 15(5):4912, 2014.

[50] Rogers DWO, Faddegon BA, Ding GX, et al. "BEAM: a Monte Carlo code to simulate radiotherapy treatment units." *Med Phys.* 22(5):503–524, 1995.

[51] Wulff J, Zink K, Kawrakow I. "Efficiency improvements for ion chamber calculations in high energy photon beams." *Med Phys.* 35(4):1328–1336, 2008.

[52] Seltzer SM, Fern andez-Varea JM, Andreo P, et al. "Key data for ionising radiation dosimetry: measurement standards and applications" *ICRU Report 90*. Oxford: International Commission on Radiation Units & Measurements (ICRU); 2016.

[53] British Institute of radiology “Central Axis Depth Dose Data for Use in Radiotherapy Departments” *BJR Supplement 25*, BIR, London, 1996.

[54] Dufreneix S, Ostrowsky A, Rapp B, Daures J and Bordy J-M “Accuracy of a dose-area product compared to an absorbed dose to water at a point in a 2 cm diameter field” *Med. Phys.* 43:4085-4092, 2016.

[55] Djouguela A, Harder D, Kollhoff R, Rühmann A, Willborn KC, Poppe B “The dose-area product, a new parameter for the dosimetry of narrow photon beams.” *Z Med Phys.* 16:217–227, 2006.

[57] Zoros E, Moutsatsos A, Pappas EP et al. ”Monte Carlo and experimental determination of correction factors for gamma knife perfexion small field dosimetry measurements.” *Phys. Med. Biol.* 62(18): 7532, 2017.

[58] Looe HK, Büsing I, Tekin T, et al. ”The polarity effect of compact ionisation chambers used for small field dosimetry.” *Med Phys.* 5608-21, 2018.

[59] Gul A, Fukuda S, Mizuno H, et al. “Feasibility study of using Stereotactic Field Diode for field output factors measurement and evaluating three new detectors for small field relative dosimetry of 6 and 10 MV photon beams.” *J. Appl. Clin. Med. Phys.* 21(11): 23-36, 2020.

TURUN
YLIOPISTO
UNIVERSITY
OF TURKU

Painosalama, Turku, Finland 2025

ISBN 978-952-02-0124-1 (PRINT)
ISBN 978-952-02-0125-8 (PDF)
ISSN 0082-7002 (Print)
ISSN 2343-3175 (Online)